International
Progress Report

IPR-04-08

Äspö Hard Rock Laboratory

Using borehole tides to determine fracture parameters

1 – Theory, pre-study, and literature survey

Hans-Georg Scherneck

Chalmers University of Technology

December 2001

Svensk Kärnbränslehantering AB
Swedish Nuclear Fuel
and Waste Management Co
Box 5864
SE-102 40 Stockholm Sweden
Tel 08-459 84 00
+46 8 459 84 00
Fax 08-661 57 19
+46 8 661 57 19

Äspö Hard Rock Laboratory

Report no.
IPR-04-08
No.
F50K
Author
Hans-Georg Scherneck
Date
Dec. 2001
Checked by
Mansueto Morosini
Date
2004-05-24
Approved
Christer Svemar
Date
2004-06-11

Äspö Hard Rock Laboratory

Using borehole tides to determine fracture parameters

1 – Theory, pre-study, and literature survey

Hans-Georg Scherneck

Chalmers University of Technology

December 2001

Keywords: Earth tides, tidal strain, ocean tide loading, confined aquifers, atmospheric loading, groundwater tides, fractured rock, crystalline rocks, borehole geophysics, hydrogeology, precambrian rocks, Sweden, Baltic Shield, Äspö HRL

Abstract

The possibility to use tide observations in boreholes to determine fracture parameters is investigated. This report is the first part of two, and presents the theoretical background and a pre-study. Well tides have clearly been observed in the KAS03 borehole located at Äspö. A time series is analysed from this location. Basic concepts are developed along with a review of the relevant literature.

The second part will report the results from estimation of tidal parameters and inference of parameters of a fracture zone model, using observations from 40 different boreholes or borehole sections at Äspö.

Sammanfattning

Den här studien undersöker om det är möjligt att bestämma parametrar för sprickor ur mätningar av tidala vattentryckvariationer i djupa och täta borrhålssektioner. Studien sammanfattas i två delrapporter. Den här delen presenterar den teoretiska bakgrunden för tidal påverkan i en sprickzonsmodell samt en förstudie. Tidala tryckvariationer har observerats i borrhålet KAS03 sektion A (djup 800 m), och ett systematiskt samband med den tidala töjningen i jordskorpan framstår som tydligt. En tidsserie från denna sektion undersöks i detalj för att exemplifiera grundkoncepten, och facklitteratur med liknande frågeställningar sammanfattas och kommenteras. Del två kommer att omfatta resultat för sprickzonsparametrar när den tidala metodiken använts på ca. 40 borrhålssektioner från Äspö.

Contents

1 Aimes and scope of this study

Observation of ground water in deep boreholes, particularly in crystalline rock often reveal variations with a clear tidal behaviour. This means that changes in water head follow with the moon and the sun in roughly the same way as the ocean surface does, which is the familiar phenomenon of ocean tides. Depending upon observation conditions, the borehole signal appears in the form of pressure changes (e.g. in packed sections of boreholes); in water head changes in deep, but open boreholes; in strain that can be measured as small borehole caliper variations, and even in flow variations in drained wells. Whereas pressure changes may amount to several tens of centimetres, strain measurement would call for special transducers as these effects are only a few parts in 10^9.

The tidal effect is most convincingly explained by the fact that the earth crust is strained as the tide raising bodies deform the earth. Under the uplifted part of the tidal bulge the crust is stretched in extension. Pore volumes are easier stretched than the rock matrix, thus pore volume increases and water pressure sinks. A connected network of cracks will facilitate pressure equilibration in a large or eventually even the total volume of rock. Under reasonable confinement, the pressure change will affect only a certain volume, and this volume might include a probing borehole. The confinement might be dissipative as time goes on, so that, if the strain change would persist at a constant level, the pressure would equilibrate (with the atmosphere as the final end state).

As we have noted and what will be shown in this report, tides in ground water in crystalline rock has an important similarity with ocean tides, at least in a superficial view. The exact time of highest level does not directly correspond to the maximum gravitational pull of the tide raising celestial bodies. Also, the amplitude of the locally observed water tide has no direct relation to the maximum gravitational pull. In each case, modifying transfer properties come into play. In the case of the ocean tide it is the phenomenon of resonance of a basin, reminding of the oscillations of a bath tub. If the excitation frequencies are not substantially different from the natural resonance frequencies, passive resonance leads to complicated amplitude and phase relations between “input” (tidal gravity pull) and “output” (observed water height). In aquifers friction is comparatively high and volumes are small, so that resonance would occur only at very high frequencies, if at all; frictional and inertial effects would affect only the response at seismic frequencies (Mavko and Mukerji, 1995). Instead, the elastic response of an oriented crack in a finite network of fractures is thought to be responsible for the observed amplitude, and the complex coupling of the different components of strain are responsible for the phase. This will be explained in detail in the theory chapter of this report. The crack, however, will generally by leaky, i.e. slowly drain to cracks with different orientation and different properties, and ultimately to the atmosphere.

Thus, aquifer confinement, rock matrix elasticity, fluid compressibility, aquifer transmissivity into the borehole, and the orientation of cracks somehow matter in the process from imposed tidal deformation to observed pressure change. The method has earlier been used successfully by Hanson and Owen (1982), Bower (1983) and Endom and Kümpel (1994).

1.1 Aims

Observation of fractures in crystalline bedrock is an important subject in conjunction with waste disposal (e.g. Tiren et al., 1999). Since borehole tides are easily observable in ground water pressure or water head, provided the pore filling water volume is not disturbed by pumping etc., the question arises whether these relations could be used to probe certain parameters that may help characterize boreholes and/or rock masses. By correlation with (hydro-) geological parameters one might be able to derive a rather cost-efficient exploration method. This would be applicable primarily in deep boreholes, where other methods have difficulties with resolution (e.g. radar, Wanstedt et al., 2000). In this aspect we are going to penetrate a new area of applied geoscience, with an uncertain outcome at the outset.

The present work draws from several fortunate or practical circumstances. Geosigma has developed a method to sense water pressure in rock via boreholes, in which the transmissivity into the borehole is negligible. The method employs packers that isolate short sections of borehole, and pressure is directly sensed by transducers rather than through water head variations. Thus, flow is kept at a minimum. Also, there are long records of pressure measurements available where the tide response method can be studied.

The primary aim with this first part of the study is to try and analyse tides in one borehole as a pilot case. The record that is analysed has been selected for favourable conditions as concerns length, sampling interval, resolution, noise, and a low number of perturbing events.

In a second volume, a large number of records from different borehole sections will be analysed employing the methods and relating to the concepts that are laid out in this, the first one of a two-volume report.

1.2 Scope

This volume will discuss the theory of deep ground water tides in fractures of crystalline rock. The primary tide effect is strain, and it is thought be composed of the luni-solar generated strain and the slightly smaller effect due to ocean tide loading. After the theory has been introduced, an example for its application is shown. Analysis of borehole pressure records is carried out in terms of tidal parameters, which are interpreted in terms of hydraulic parameters and fracture orientation angles in the next step.

Finally, in two appendices, the existing analysis software and the literature in the field are provided.

2 Theory of tides in fluid-filled fractures of the crystalline bedrock

The notion of water head variations in wells is old. The most well-known effect is the influence of **varying air pressure** that drives water to flow from the well bore into the aquifer. The response is mainly dependent on the well bore, the aquifer's hydraulic conductivity and storage capacity, but is modified also by the influence of the air pressure on the aquifer itself. Some aquifers are more or less decoupled from the atmosphere by overlying layers of rock (solid crystalline, sediment), so the atmospheric load can put a direct counterweight on a column of water in the aquifer. The confined conditions are characterised by the strain that the rock matrix and the network of fluid-filled or partially fluid-filled voids are undergoing. Due to the relations of compressibility between the matrix and the filling the pore pressure will vary and thus influence the fluid flow. For this reason almost all kinds of aquifers show barometrically induced tides, even in those cases where the well itself is closed off from the atmosphere. This group of aquifers comprise also the kind applying to this study, fluid-filled fractures in deep rocks.

The **response of aquifers to tides** is controlled by the strain of the rock matrix. It is similar to the response of an aquifer to passing seismic waves, however occurring at very-low frequencies. At low frequencies flow and diffusion effects can be significant, but the inertia of the water can be neglected. For the tidal effect differential gravity forces on the water and the surrounding rock are only of secondary importance. In open aquifers (where strain is inefficient to generate fluid pressure change) the tidal attraction of moon and sun and the secondary gravity effects of the deforming earth would generate only a small tidal tilt of the water surface (less than 0.05 arc seconds or 0.25 millimetre level change over one kilometre. It would therefore require a band-pass filter effect, for instance a certain well bore geometry to coincidentally cause interaction with the aquifer with a resonance at a tidal frequency, so that the effect would become directly visible. The negative findings implied by e.g. De Vries and Gieske (1988) and work by Delcourt-Honorez (1986, 1991) support the notion that tides are more likely to be found in confined aquifers. The literature survey (Chap. 5.2) shows many examples. The presence of tides is sometimes used to conjecture confined behaviour (Larocque et al, 1998). An exception is found in coastal unconfined aquifers in high-tide regions (Robinson and Gallagher, 1999). Rojstaczer and Riley (1990) derive the conditions under which tides would emerge at a noticeable level, namely very high hydraulic conductivity and very low specific yield; also the aquifer thickness must exceed the diffusive depth, i.e. unrealistically thick aquifers.

Thus, the existence of tides in fluid-filled voids in rock is primarily a consequence of the strain of the rock. A borehole that penetrates a fracture will drain the fracture. Modified to a certain degree by confinement conditions, the pressure in the fluid of the borehole will depend on the fluid pressure in the void. Thus, borehole fluid pressure becomes an indicator of strain around the fracture and the response of that fracture to the strain. One source of strain which has the favourable property of stationarity is the strain of the earth as it deforms under the gravitational pull of the celestial bodies, the earth tides. This process is regular and can be predicted with very high accuracy.

This report will utilise these relations to determine parameters characterising the fracture. The analysis is based on ground-breaking work by Hanson and Owen (1982), Hanson (1983) and Bower (1983) It proposes to use modern time-series analysis procedures, specifies methods to compute the astronomical effects, and considers three sources of tides in ground water pressure in confined aquifers, solid earth (oceanless earth) tidal strain, ocean tide loading strain and atmospheric pressure loading-induced strain.

This report tries to answer **what fracture parameters can be addressed in an analysis of borehole tides in sparsely fractured rock, optionally augmented with barometric response.** This application is not new as the literature references indicate, and it has recently been applied in a case study (Endom and Kümpel, 1994). The high quality that tide records can reach if sampling conditions are favourably exploited can be very high, so high that new findings about so remote features as the earth's core can be explored (Zaske et al. 2000).

The basic principle is the following:

1. Tidal forces due to moon and sun strain the earth crust.

2. Using stress-strain relations one can compute stress on a planar fracture.

3. The normal stress on the fracture and, with a much smaller coefficient, also the tangential stress are related to the pressure of a liquid that fills the fracture. The orientation of the fracture with respect to the principal directions of the strain field determines the amount by which the fracture is widened or narrowed.

4. There are three independent components in the tide strain. The ratios between the horizontal components are unique in each fundamental tide band (semidiurnal, diurnal, etc.).

5. As a consequence of the stress-strain relations and the orientation of the fracture, the pressure in the filling of the fracture is a specific, quantifiable mixture of the stress components. The mixture is unique in each fundamental band. It is dependent on the latitude of the station.

That is, semidiurnal and diurnal tide amplitude parameters are mainly indicative of a strike direction of a fracture. A dip angle can be computed if the elastic parameters of the rock and the hydraulic coupling between stress in the rock and pressure in the borehole are known within reasonable bounds. The wide-band frequency response can be used to constrain this relation further. The precision with which the dip angle can be determined improves if the air pressure response of the bedrock unit is included.

ad.4: Concerning the most familiar effects, the earth is deformed globally according to a tesseral function at periods near one cycle per day and according to a sectorial function near two cycles per day. Most importantly, NE-shear is at phase quadrature with the NN and EE components. Section 2.2 shows details.

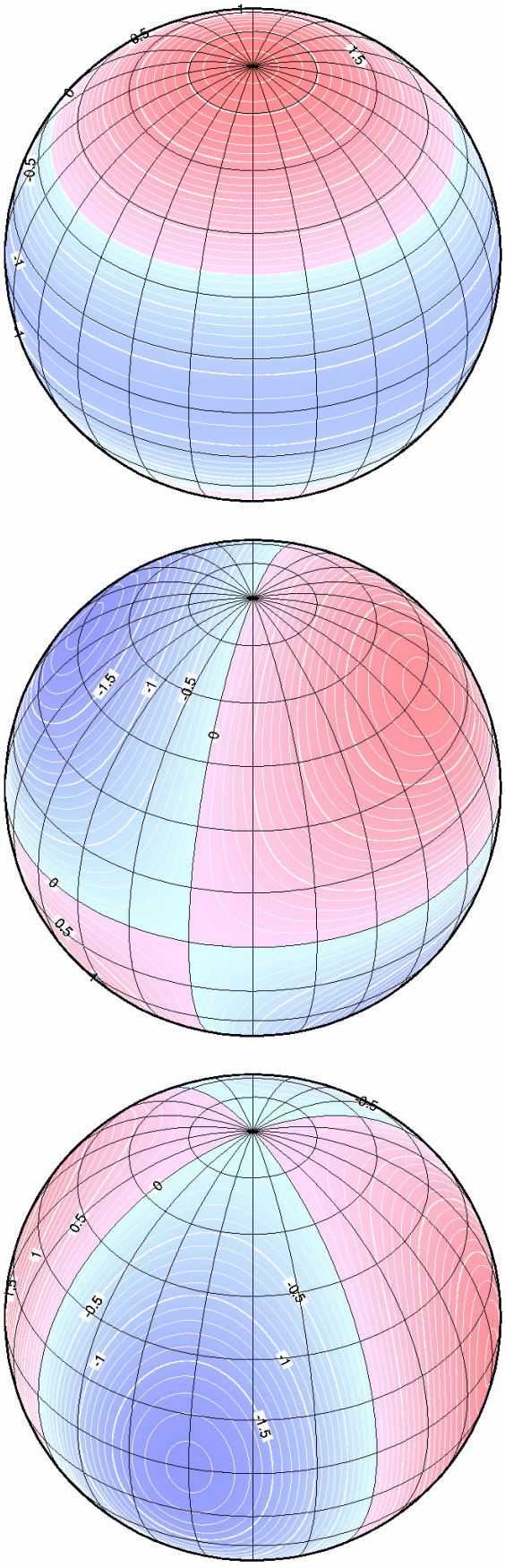

Figure 2-1. *The three kind of solid earth tides (principal effects of spherical harmonic degree two). Top: Zonal harmonic, pertaining to spherical harmonic order zero, long-periodic effects. Middle: Tesseral harmonics, order one, diurnal effects. Bottom: Sectorial harmonic, order two, semidiurnal effects. Areal strain and vertical displacement are proportional to the field displayed, horizontal displacement to the gradient*

ad.5: Comparison between the fracture response at diurnal and semidiurnal periods provides enough constraints to invert the response and estimate dip and strike angles for a planar fault.

For a deeper understanding sections in the final report will be devoted to gain the necessary insight into the tidal deformation of the earth, the homogeneous earth tide strain field, and the impact of stress on a planar fracture in the crystalline crust.

The report is organised as follows. First the prerequisites for an investigation of borehole tides are given. Next, the theory is reviewed. With theory, observed data and software in place, a report of analysing almost 6 months of hourly data from a borehole on Äspö is given. The third part of the report gives a review of literature concerning the relation between tides and ground water pressure and some additional work that is of potential importance for the work. The emphasis in this report is to devise a least complicated analysis scheme that can be used by technical staff to obtain fracture parameters.

2.1 Prerequisites for investigation

The investigation will make use of tides for a number of advantageous properties. Primarily, tides are characterised as a stationary, bounded signal which can accurately be approximated with a finite number of sinusoids. Thus, harmonic analysis applies, and a large number of methods are at disposal that focus on the problem to discern harmonic signals in noise. Also, tides are deterministic, i.e. accurately predictable. Limitations in these properties have an almost academic notion.

2.1.1 Observation data

The main sources of data for this investigation are **pressure measurements in packed sections of a borehole**. The follow-up study aimed at probing for quality parameters for such measurements. A priori, drawing from experience in tide analysis a short overview is given in Table 2-1.

Basically, the RMS of the data noise is proportional to the size of the confidence limits in the data. The length of the time series decreases the signal to noise ratio with the square-root of the number of samples. The spectral separability of tidal waves, which is required to discriminate between lunar and solar effects, demands that one month is a minimum time window for observation. The Nyquist theorem demands that the longest permissible time interval in earth tides is 4 hours.

If the data noise is irregular, use of more extensive filtering and data rejection will decrease the signal to noise level further.

Table 2-1. Time series properties and consequences. Typical values are shown in parenthesis, crucial limits appear in fat style.

Property	**Consequence**
Duration of observing interval (**14 d** - 180 d)	short: data processing advantage; efficient production of results.
	long: improved frequency resolution
Sampling rate (0.1 - **3 h**)	low: aliasing
	high: improved signal to noise ratio
Measurement resolution (0.1 - **10** mm WH)	precision of parameter determination
Noise correlation and rich power spectrum colour	urges filtering and data edition, leading generally to lower SNR, higher parameter uncertainty, and correlation between estimated parameters.
Gaps	degrade frequency resolution
	limit applicability of spectrum analysis tools

2.1.2 Model predicted data

Earth tide **strain** can be computed from models. In continental interior the largest component is due to the solid earth tide. The presence of ocean tides adds a more complicated strain field. At large distance from the major tidal basin this field can be computed with reasonable accuracy from global ocean tide models. Both solid earth tides and ocean loading tides can be characterised with a limited number of time-invariant parameters. Thus, the underlying model can be computed once-for-all, and time series of modelled strain can be computed conveniently (i.e. without the need to acquire specific data).

Other sources of strain in the crust are nontidal changes of water levels in large lakes and sea basins in the region with the crustal loading and deformation problem ensuing; changes of air pressure; changes of soil moisture; snow cover; tectonic transients; possibly “quiet” earth quakes; thermal changes etc. One group of effects is particularly perturbing, namely those that are synchronous with the sun (as a consequence of solar radiation and surface heating), and those correlated with annual climatic cycles, which usually generate a suite of upper harmonics (semi-annual etc.). From these considerations it becomes clear that very long time series are ideal for the separation of solar and lunar effects, and the identification of annual changes from long-term trends might also turn out useful in studies to identify causes and effects.

2.1.3 Ancillary observations

Additional observations are required to support models of external influences. Due to their variability **air pressure** and **sea levels** are the most important processes in this context. Typically, tidally induced pressure in fluid-filled voids reaches levels of tens of hektopascal. Barometric pressure variation is in the same order of magnitude. A sea area near a borehole site (actual example: the Baltic Sea near Äspö) might undergo level

changes of ±0.3 m. This relates to bottom pressure changes of tens of hektopascal, i.e. at the same level as barometric variations. It is through the geometry of the load that strain underground is induced more or less efficiently. This PM will show that the tides in the North Atlantic have a significant loading effect in south-east Sweden. Correlation between the Baltic Sea level and borehole pressure is also found. As already indicated above, I will try and use relations between surface air pressure and water level to add constraints in the inversion for fracture parameters.

2.1.4 Methods

Tide analysis, least-squares adjustment of a linear model to observed data; see Section 2.2.1 for details.

Spectral noise-whitening methods, like Burg's Maximum Entropy construction of prediction-error filters; see Section 2.4.1 for details.

A parameterised model of the fracture zone; see Section 2.3 for details.

Non-linear least-squares adjustment of the parameters of the fracture zone model; see Section 2.3.3 for details.

Tide synthesis, usually a subsystem of tide analysis; see Section 2.2 for details.

Cross-spectrum estimation, including Wiener filter construction; see Section 2.4.2 for details.

2.2 Earth Tides

Without lengthy derivation we note the following representation of tide displacement of a point at the earth surface in vertical (u), east (v) and north (w)

$$u = \sum_k \frac{h_{n(k)}}{g} H_k P_{n(k)}^{m(k)}(\cos\vartheta)\cos[\chi_k + \omega_k(t-t_0) + m(k)\lambda] \quad (2\text{-}1a)$$

$$v = -m\sum_k \frac{l_{n(k)}}{g} H_k P_{n(k)}^{m(k)}(\cos\vartheta)\sin[\chi_k + \omega_k(t-t_0) + m(k)\lambda] \quad (2\text{-}1b)$$

$$w = \sum_k \frac{l_{n(k)}}{g} H_k \frac{\partial}{\partial\theta} P_{n(k)}^{m(k)}(\cos\vartheta)\cos[\chi_k + \omega_k(t-t_0) + m(k)\lambda] \quad (2\text{-}1c)$$

from which strain can be computed by partial derivatives with respect to spherical co-ordinates, co-latitude ϑ and longitude λ. The amplitude coefficients H_k are in gravity potential units (m^2s^{-2}). Tables are available for $H, n, m, q_2, q_3, q_4, q_5, q_6, q_7$, (e.g. Hartmann and Wenzel, 1995). The phases and frequencies are computed from the astronomical arguments τ, s, h, p, N, p_s (lunar time, tropical month, tropical year, lunar perigee, lunar node, and perihelion) for which formulas are available, normally in software that accompanies the tide table. The astronomical arguments are functions of Terrestrial Time T (TAI + const.) which is related to UTC through the familiar leap seconds. The following relation between mean lunar time τ, mean solar time t (~ UTC), and sidereal time θ holds

$$\theta = \tau + s = t + h$$

The tide argument for an instance of time is computed by

$$\chi_k = m\tau + q_2 s + q_3 h + q_4 p + q_5 N + q_6 p_s + \tfrac{\pi}{2} q_7 \qquad (2\text{-}2)$$

at time t_0 and the angular velocities are

$$\omega_k = \frac{d}{dt}\chi_k$$

almost constant. Quite analogously the tide gravity potential due to the tide raising bodies can be described by

$$\Psi = \sum_k H_k P_{n(k)}^{m(k)}(\cos\vartheta)\ \cos[\chi_k + \omega_k (t - t_0) + m(k)\lambda] \qquad (2\text{-}3)$$

The functions $P_{n(k)}^{m(k)}$ are Associated Legendre functions (see e.g. Arfken, 1985). For nonzero terms, $0 \le m \le n$. The largest tides are due to degree n=2, cf Figure 2-1. Owing to the distance of the moon, 60 earth radii, the lunar tides of the next degree are smaller by the order of magnitude of 1/60, and the solar species are totally negligible already at n=3. Of all arguments, $m(\tau + \lambda)$ is dominant (lunar time with one period per 25 hours plus station longitude), and m can be zero (long-period tides), one (diurnal tides) and two (semidiurnal tides). The tide spectrum of the gravity potential is shown in Figure 2-2.

> The most familiar tide, the lunar principal tide M_2 has n=m=2 and all q's are zero. This tide that has exactly two crests per lunar day, one when the mean moon transits the local meridian, and one exactly in the middle of two consecutive transits, when the moon is at the transit antipode.

The earth's response in terms of vertical and horizontal displacement is characterised by the so-called Love numbers, h_n and l_n, respectively. For orientation I give some general numeric values for the Love numbers in Table 2-2. More details can be obtained from Wahr (1981), especially concerning the strong frequency dependence of the numbers for (n, m) = (2, 1) around the resonance period 1 cycle per 1+1/435 days.

I add the formulas for computing strain from displacement in spherical co-ordinates,

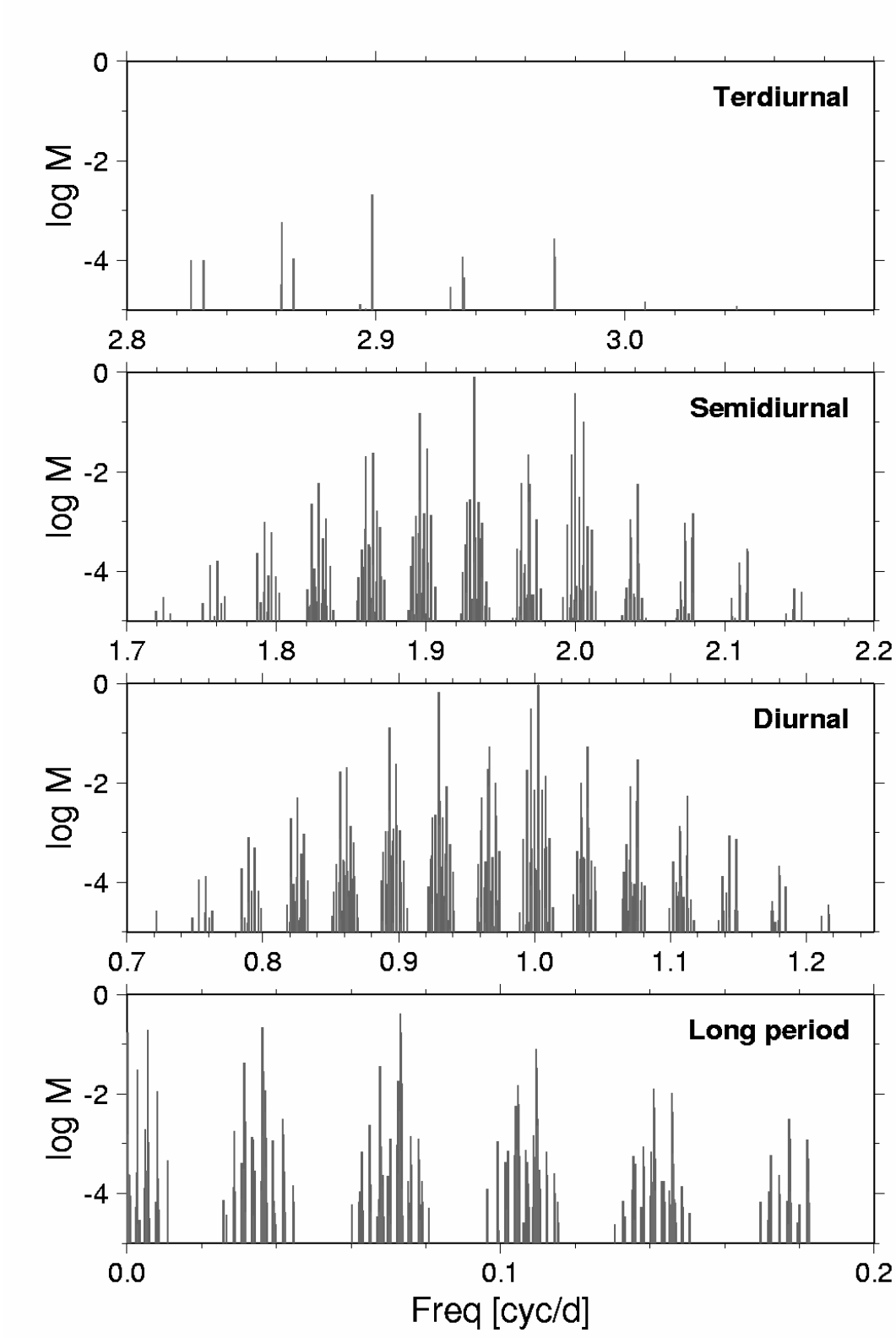

Figure 2-2. *Tide spectrum, distinguishing between the different fundamental frequency bands. The species leading in amplitude and shown in black correspond to spherical harmonic degree 2, the species shown in blue correspond to spherical harmonic degree 3 and are about 1/60 smaller (since the moon's distance is 60 earth radii). Each band has a structure of 2 beat periods per month as an effect of lunar orbit inclination and ellipticity.*

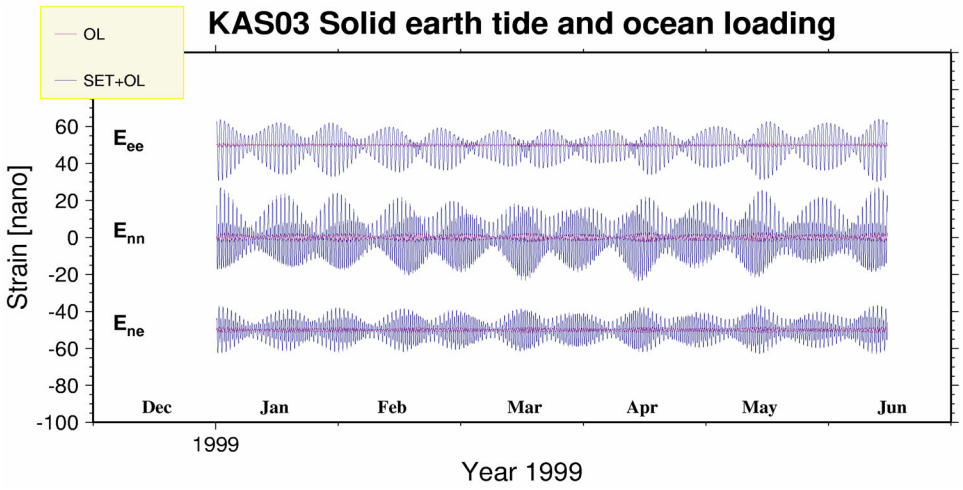

Figure 2-3. *The solid earth tide (blue) and ocean loading tide (red) computed in the horizontal strain components for the site Äspö.*

$$\varepsilon_{ee} = \frac{\partial v}{r \sin\vartheta \, \partial\lambda} + \frac{u}{r} + \frac{w}{r \tan\vartheta}$$

$$\varepsilon_{nn} = \frac{\partial w}{r \, \partial\vartheta} + \frac{u}{r} \qquad (2\text{-}4)$$

$$\varepsilon_{ne} = \tfrac{1}{2}\left(\frac{\partial w}{r\partial\vartheta} + \frac{\partial v}{r \sin\vartheta \partial\lambda} - \frac{w}{r}\cot\vartheta \right)$$

Time series are shown in Figure 2-2. Near the earth's surface, where the boundary is stress-free, the vertical strain components are zero, except

$$\varepsilon_{zz} = \frac{-\lambda}{\lambda + 2\mu}(\varepsilon_{ee} + \varepsilon_{nn}) \qquad (2\text{-}5)$$

where λ and μ are the elastic moduli (Lamé-parameters). For convenience the equations (2-1) can be written

$$u = \mathrm{Re} \sum_k U_k \exp[i\omega_k (t - t_0)] \qquad (2\text{-}6)$$

and equivalently for v and w, with complex tide coefficients U_k etc. This extends to strain components

Table 2-2. Love numbers. Values quoted from Wahr (1981) and Farrell (1972)

n,m	h	l
2,0	0.606	0.0840
2,1	0.603	0.0841
2,2	0.609	0.0852
3,*	0.289	0.0145

$$\varepsilon_{rs} = \mathrm{Re}\sum_k \mathrm{E}_{rs,k}\ \exp[i\omega_k (t - t_0)] \qquad (2\text{-}7)$$

Remark on symbols: capital letters like the Epsilon above denote spectrum coefficients, lower-case the time domain equivalent. The subscript *k* denotes a (enumerated) spectral line, and the subscripts *rs* address the strain tensor component.

With the definitions of the harmonic sums, the properties of the solid earth tide displacement field (2-1), and the strain derivatives (2-4) it is not difficult to see that for diurnal tides and higher period tides (i.e. $m>0$)

$$|\arg\frac{\mathrm{E}_{ne,j}}{\mathrm{E}_{ee,j}}| = 90^o, \quad |\arg\frac{\mathrm{E}_{ne,j}}{\mathrm{E}_{nn,j}}| = 90^o$$

Finally borehole pressure will be written

$$p_w = \mathrm{Re}\sum_k \Pi_k\ \exp[i\omega_k (t - t_0)] + p_{nontidal} \qquad (2\text{-}8)$$

Analysis of tides in wells tapping porous media or tides measured in fluid pressure in fractures in crystalline rock starts from tide strain, rather than stress. The reason is that the relatively thick mantle controls the strain of the relatively thin crust, and stresses form in order to keep the materials in contact. There is usually not much variation in the Poisson coefficient, materials are isotropic at least at the first order of deformation, and the material is undergoing tidal stress cycles which are usually far uncritical with respect to material strength. This also holds for atmospheric loading, for which a more rigorous account is given in Rojstaczer and Agnew (1989). The regional areal strain due to tides or air pressure loading can be computed using global parameters. The pressure in the water-bearing structure is related to this strain by local parameters like the formation's compressibility.

2.2.1 Tide analysis

An observed time series can be decomposed into tidal components and a nontidal residual. To that end the sum in (2) is removed. To compute one response parameter for each wave, however, is not possible in a situation of finite-length observations. For example a time-series that is 1/2 year long allows only safe discrimination of effects that differ in the tide argument by at least $2h$. If a time series is less than 14 days long, lunar and solar effects become hard to separate. Therefore, wave-groups are formed according to the frequency resolution capability that is compatible with the observation window. Anticipating degree- and order-dependent response parameters (i.e. pertaining *n* and *m*), the wave-groups are not to mix terms with different *n* and *m*. Finally, response parameters u_j for the wave groups are determined using least-squares procedures.

$$\Psi_{tj} = \sum_{k=K(j)}^{L(j)} H_k P_{n(k)}^{m(k)}(\cos\vartheta)\ \exp \mathrm{i}\,[\chi_k + \omega_k (t\,\Delta t - t_0) + m(k)\lambda] \qquad (2\text{-}9)$$

Pressure and potential time series for Äspö are shown in Figure 2-4.

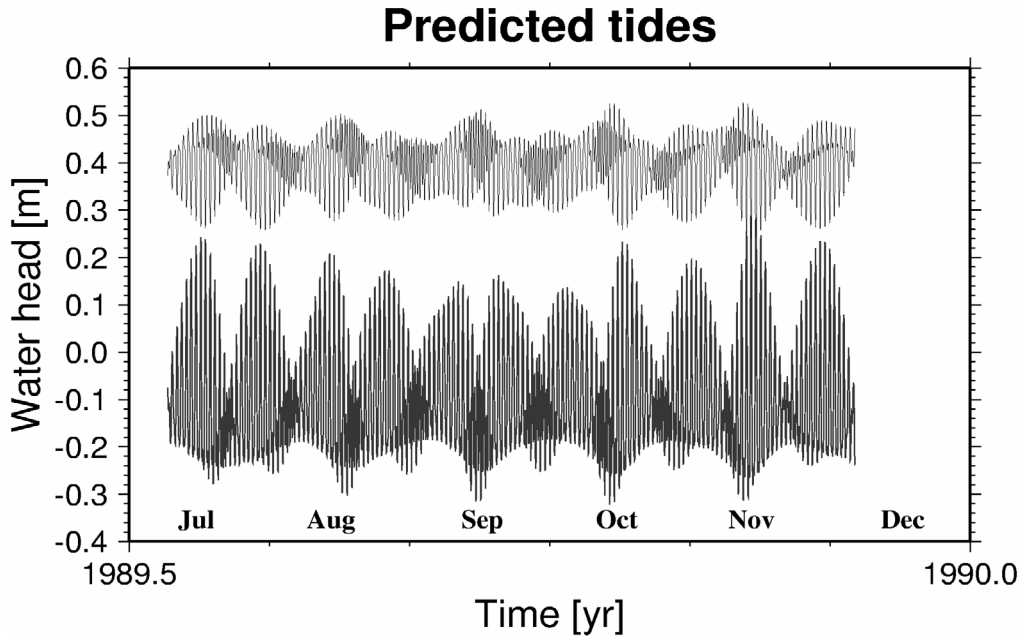

Figure 2-2. *The water pressure tide in the KAS03 borehole (top) predicted from the result of the least squares tide analysis. Shown is also the gravity potential for the same location and time (bottom).*

$$\sum_j \Psi_{tj} \tilde{U}_j = y_t + \delta_t, \qquad \delta^T \mathbf{V}^{-1} \delta \overset{!}{=} \min$$

where δ is the error of the fit and **V** the data covariance matrix, and the tilde symbols denote complex **admittance coefficients.** The wave-group approximation of e.g. observed pressure is then

$$p = \sum_j \Psi_{tj} \tilde{\Pi}_j + \delta_t \qquad (2\text{-}10)$$

with admittance coefficients $\tilde{\Pi}_j$, and likewise for inferred or predicted strain

$$\varepsilon_{rs} = \sum_j \Psi_{tj} \tilde{\mathrm{E}}_{rs,j} + \delta_j \qquad (2\text{-}11)$$

where the sums run over the wave-groups as in (2-9). Knowing p and ε_{rs} from observations respectively prediction, we can define **strain coupling parameters** as follows:

$$p = Q * (\alpha_1 \varepsilon_{ee} + \alpha_2 \varepsilon_{nn} + \alpha_3 \varepsilon_{ne}) \qquad (2\text{-}12)$$

where Q is a transfer function that accounts for dispersive effects (frequency dependent response). The corresponding wavegroup relation is then

$$\tilde{\Pi}_j = Q(i\omega_j)(\alpha_1 \tilde{\mathrm{E}}_{ee,j} + \alpha_2 \tilde{\mathrm{E}}_{nn,j} + \alpha_3 \tilde{\mathrm{E}}_{ne,j}) \qquad (2\text{-}13)$$

where the coupling parameters are supposed to be **frequency-independent**. The final modification of this scheme is the combination of the diagonal strain elements to separate the expression into a “normal” areal strain component and two deviatoric components

$$\tilde{\Pi}_j = Q(i\omega_j)\left[\beta_1(\tilde{E}_{ee,j}+\tilde{E}_{nn,j})+\beta_2(\tilde{E}_{ee,j}-\tilde{E}_{nn,j})+\beta_3\,\tilde{E}_{ne,j}\right] \qquad (2\text{-}14)$$

More details on Q are given in Section 2.3.1.

2.2.2 Ocean loading tides

While solid earth tides can be computed with a relatively simple, globally valid formula, owing to the fact that the geographic variation is almost fully described by two hands full of spherical harmonics, the effect of ocean tides is a bit more difficult to describe. The geographic distribution of the strain is controlled by the tides in ocean basins; the effect decreases into the continents, but does not drop to zero, cf Figure 2-5. The relation between the tide in the ocean and the deformation anywhere in the earth and along the earth surface can, however be reduced to a quite simple form.

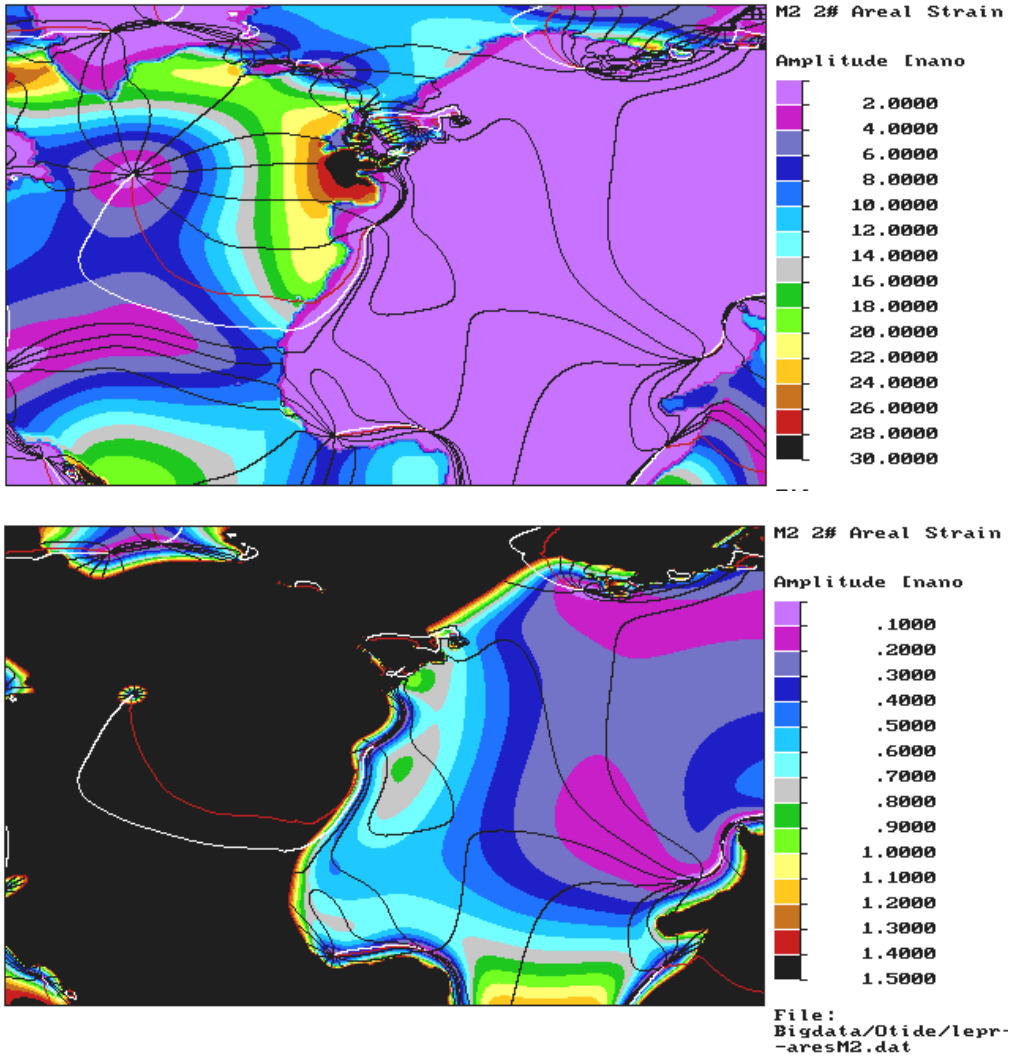

Figure 2-3. *Ocean loading effect, areal strain due to the M_2 global ocean tide. The Le Provost et al. (1994) has been employed. The top frame shows an amplitude range up to 30 nano, suitable for oceanic regions. The bottom frame enhances the range below 1.5 nano.*

The influence of a point mass loading the crust at a location (latitude, longitude) = (Θ, Λ) upon an effect of deformation at another point (θ, λ) can be described with a Green's function. The effect of all loading masses is then described by an integral that sums up all masses multiplied with the Green's function G (cf Farrell, 1972; Scherneck, 2001). This is an operation called global convolution with as an integrating kernel

$$\xi(\theta,\lambda) = \int_O \mathsf{G}_\xi(\theta,\lambda;\Theta,\Lambda)\rho\zeta(\Theta,\Lambda)\,d\Sigma(\Theta,\Lambda) \qquad (2\text{-}15)$$

Here, ρ is the density of sea water, ζ the tide height, $d\Sigma$ a surface element of the ocean, the integral extends over the Ocean O, and the result is a deformation effect, where the generic symbol ξ may stand for *u, v, w* etc.

In an earth with radially symmetric layering the Green's function is independent on the explicit position of load and field points, but only dependent on their distance. I have denoted the distance as the angle φ on the great circle arc connecting (Θ, Λ) and (θ, λ).

$$\xi(\theta,\lambda) = \int_O \mathsf{G}_\xi(\varphi)\rho\zeta\,d\Sigma \qquad (2\text{-}16)$$

At the field point let the azimuth (clockwise from north) of the connecting arc be denoted by α. The Green's functions for vertical displacement and for horizontal displacement along direction $\hat{\alpha}$ are computed from load Love numbers h'_n and l'_n, and the strain components can be obtained using equations (2-4) and (2-5).

Since ocean pressure loads the crust without surface shear the horizontal components of strain of the unloaded crust has only two independent components, along and across the arc direction. Then the strain tensor due to surface loading is obtained by

$$\bar{\bar{E}} = \int \mathbf{T}\mathbf{G}\mathbf{T}^{\mathrm{T}}\rho\zeta\,d\Sigma \qquad (2\text{-}17)$$

where

$$\mathbf{T} = \begin{pmatrix} \cos\alpha & \sin\alpha \\ -\sin\alpha & \cos\alpha \end{pmatrix} \quad and \quad \mathbf{G} = \begin{pmatrix} \mathsf{G}_{aa}(\varphi) & 0 \\ 0 & \mathsf{G}_{xx}(\varphi) \end{pmatrix} \qquad (2\text{-}18)$$

and subscripts *aa* and *xx* signify the along-arc (or normal) and across-arc (or transverse) strain Green's functions. The resulting strain components are readily obtained for a north-east local coordinate system.

These two functions and their sum, which is identical to the areal strain function are shown in Figure 2-6. Since the functions have a singularity at zero distance, the asymptotes

$$\frac{G}{2ga^2\sin^2(\varphi/2)}$$

have been divided out (G - gravitational constant, g - mean gravity at the surface, a - equatorial radius).

The ocean loading induced strain can be added to the solid earth tide strain components given by equation (2-11). Very conveniently, ocean tide models provide gridded values for tide height and phase lag individually for a set of major tide waves (e.g. Le Provost et al., 1994; Ray, 1999). Let such an amplitude-phase pair at node (Θ_j, Λ_j) and tide constituent k be denoted by

$$Z_{kj} = A_{kj} \exp[-i\Phi_{kj}]$$

Then Z_{kj} can be substituted for ζ in equation (2-17), and the integral is replaced by a sum over all ocean nodes j. Finally, in order to add the resulting

$$\bar{\bar{\mathrm{E}}}_k = \begin{pmatrix} \varepsilon_{nn} & \varepsilon_{ne} \\ \varepsilon_{ne} & \varepsilon_{ee} \end{pmatrix}_k$$

to the strain coefficients in the wave-group equation (2-11) we have to normalise by dividing with the potential coefficient of the wave that is the dominating effect in the respective tide band

$$\tilde{\mathrm{E}}_{rs,k} = \varepsilon_{rs,k} / H_k \qquad (2\text{-}19)$$

The potential coefficients appeared first in equation (2-1). Ocean loading coefficients for Äspö are given in Table 2-3.

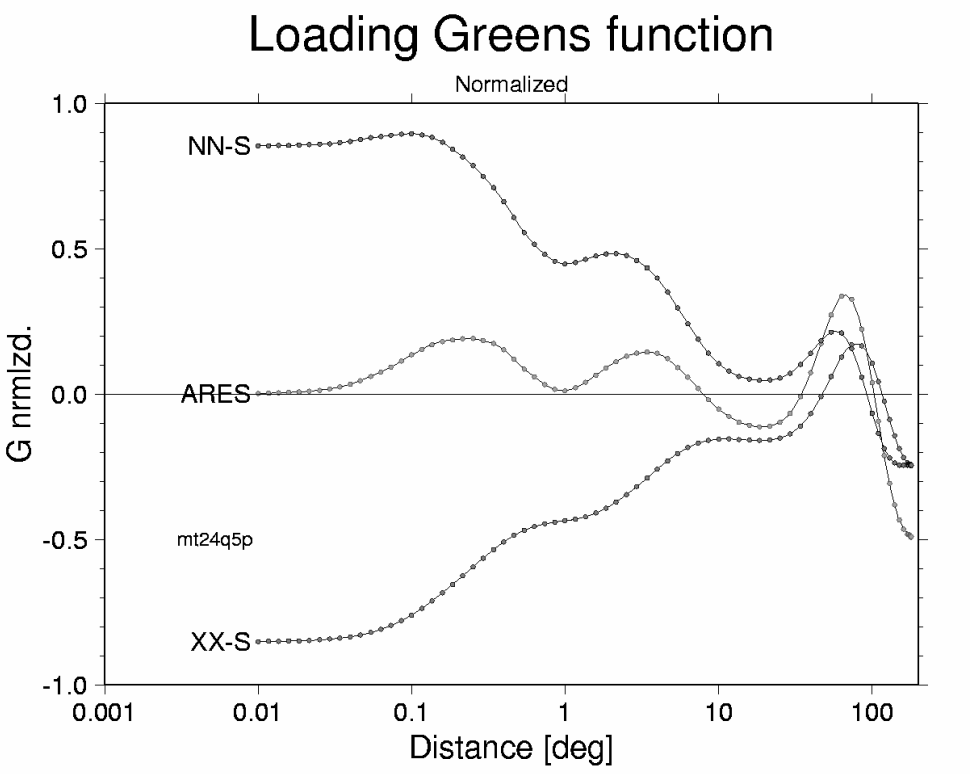

Figure 2-4. *Green's functions for the surface point load problem, shown for the components strain in the normal direction, curve labelled "NN-S" (load to field point), transverse component "XX-S" and their sum, which is identical to areal strain "ARES", a scalar variable.*

Table 2-3. Ocean loading parameters for Äspö. Amplitudes give strain in units of 10^{-6}, phases are shown in degrees of lag with respect to the astronomical tide at zero meridian.

	ε_{nn}		ε_{ee}		ε_{ne}	
	Amplitude	**Phase**	**Amplitude**	**Phase**	**Amplitude**	**Phase**
M_2	1.39	-52.1	0.56	42.0	0.93	-85.0
S_2	0.49	-15.1	0.17	-5.7	0.22	135.3
N_2	0.32	-76.1	0.17	-67.9	0.22	-98.6
K_2	0.13	-17.7	0.03	-1.0	0.07	-48.6
K_1	0.41	-42.4	0.25	133.2	0.15	138.2
O_1	0.17	-101.8	0.22	105.2	0.20	47.4
P_1	0.13	-48.2	0.09	134.4	0.05	126.1
Q_1	0.01	138.2	0.05	72.9	0.05	2.3
M_f	0.05	-10.1	0.03	-109.5	0.03	-153.3

2.2.3 Solar radiation tides

For high accuracy of the tide solution the analysis has to take into account that the tide waves with near solar frequencies (one period per solar day and the associated upper harmonics S_2, S_3 etc) might be disturbed by barometric pressure cycles. To make things even more complicated, the air pressure admittance of the borehole and the aquifer might distinguish between stochastic pressure changes at diurnal and subdiurnal periods, and the solar driven effects, since the latter might have much larger spatial coherence, and thus would be more efficient in terms of loading the crust.

For this situation it is advisable to split the barometric record into a solar part and a remainder, and to estimate gain coefficients and gain spectra separately. The frequency splitting can be done in a tide analysis stage, however now using a harmonic development of solar radiation cycles instead of the luni-solar gravity spectrum. Such a spectrum is provided by Cartwright and Tayler (1971). The time series generated for Äspö is shown in Figure 2-7. One notices the curve to resemble roughly the height of the sun above the horizon (getting lower as we get into winter), and staying near zero over night. The zero misfit is due to the few terms which are involved in the computation.

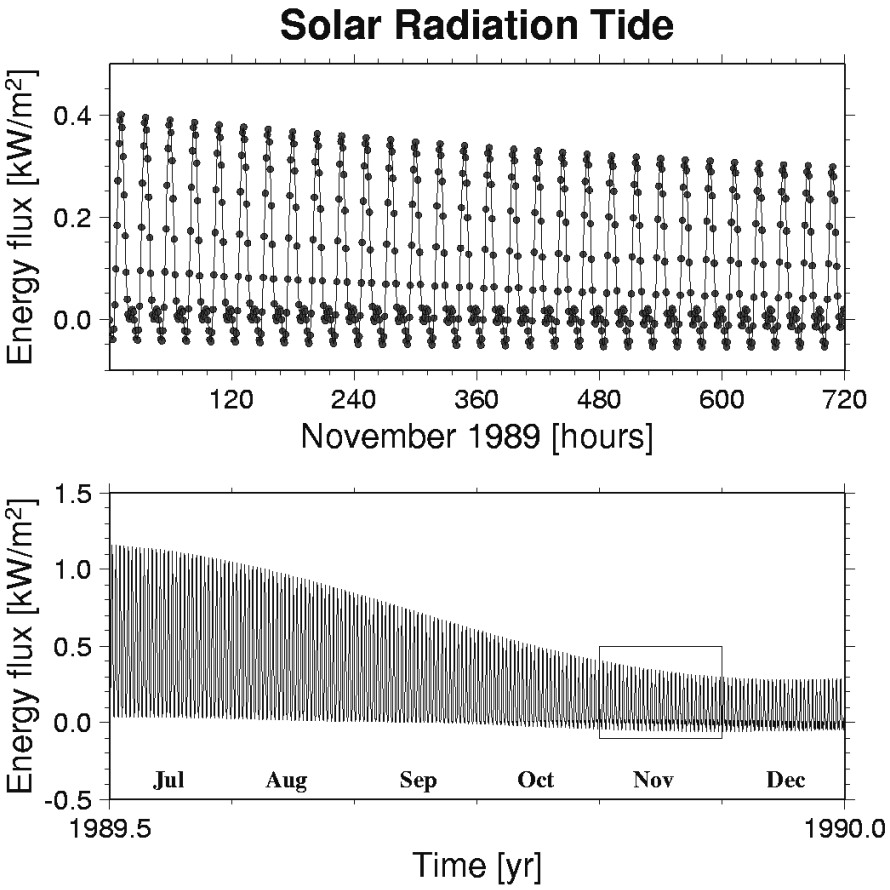

Figure 2-5. *Solar radiation "tide" for Äspö, top diagram is a blow-up of the inset in November 1989. This signal is useful for splitting the barometer record into an oscillating solar component and a stochastic remainder.*

2.3 Strain-pressure relations in fractures

The following relations are according to Bower (1983).

On a planar fracture, elastic traction normal to the fracture is transmitted and converted into fluid pressure, $p=-\tau_n$. If the fracture is finite, the tangential traction is slightly counteracting,

$$p = -\tau_n + \tau_t / E\beta \qquad (2\text{-}20)$$

where E is the Young modulus of the rock formation and β the compressibility of water. The product $E\beta$ is typically in the range of 20 to 30 (Annor and Geller, 1978). We will call it in-plane stretch ratio.

> This parameter is treated as rather heuristic in the following, since the actual shape of an asperity enters and modifies the effect of the in-plane stress. Small values of $E\beta$, however, are difficult to explain. We will encounter this problem further down in Chap. 3 when dealing with barometric loading. We might argue for thin fractures with partial contact between the walls, only a certain fraction of the rock stress would be transferred to the fluid, and an efficiency factor $0<q_{eff}<1$ would be introduced in (2-17). This makes the barometric analysis uncertain at first. But in joint analysis of tides and barometric pressure and the key parameters for elasticity of the larger geological unit given the efficiency parameter can actually be solved.

A set of finite-size voids has the capability of tide amplification since strain is prescribed and the fluid compressibility is generally lower than that of the rock matrix (Hanson and Owen, 1982). This latter work considers a vertical crack of finite dimensions with a b-wing shape, in contrast to Bowers assumptions of a penny-shaped fracture with arbitrary dip and strike orientation.

2.3.1 The tide problem

This section is for the case of negligible vertical stress, applying to tidal strain. If the fracture orientation is specified by dip D and azimuth A, then

$$\tau_n = \sigma_{nn} x_{nn}^2 + \sigma_{ee} x_{ee}^2 + \sigma_{ne} x_{ne}^2 \qquad (2\text{-}21)$$

$$\tau_t = (\sigma_{nn} + \sigma_{ee}) z^2 \qquad (2\text{-}22)$$

where

$$\begin{aligned} x_{nn}^2 &= \sin^2 D \sin^2 A \\ x_{ee}^2 &= \sin^2 D \cos^2 A \\ x_{ne}^2 &= -\sin^2 D \sin A \cos A \\ z^2 &= \cos^2 D \end{aligned} \qquad (2\text{-}23)$$

The efficiency of pressure transfer might be exaggerated with this model. In order to milder the effect we might add the pressure in a fracture of the same dip but at 90^o azimuth offset, scaled by a cross-interference factor t.b.d.

$$\tau_q = q_x (\sigma_{nn} x_{ee}^2 + \sigma_{ee} x_{nn}^2 - \sigma_{ne} x_{ne}^2) \qquad (2\text{-}24)$$

Bower's (1983) account implies q_x=0. The consequence of this assumption for the model is to mimic a fracture zone with less sharp orientation. Alternatively, the fracture might act like a thick aquifer, in effect due to contact between fracture walls, and thus transmit the rock stress to the water only to a certain fraction. This theme will be taken up again in Section 2.3.2. and in the data analysis, Section 3.2. The effect is a reduction in gain regardless how a specific strain component is coupled.

The stresses in the surrounding rock are related in a straightforward way to tidal strain, using Hooke's equations with Lamé's elastic moduli,

$$\sigma_{ij} = \lambda \varepsilon_{kk} \delta_{ij} + 2\mu \varepsilon_{ij} \qquad (2\text{-}25)$$

where we sum over repeated indices; δ_{ij} is Kronecker's delta. In the tidal problem the vertical stress components are zero

$$\sigma_{zz} = \sigma_{xz} = \sigma_{yz} = 0 \qquad (2\text{-}26)$$

and hence

$$\varepsilon_{zz} = -\frac{\nu}{1-\nu} (\varepsilon_{xx} + \varepsilon_{yy}) \qquad (2\text{-}27)$$

where Poisson's ratio ν like all the other elastic parameters is assumed to be valid for the effective rock (contemplating the fractures to be a sparse phenomenon).

Next is the question whether the pressure in the borehole is an instantaneous copy of the pressure in the aquifer, and whether that pressure has a time-invariable relation to tidal strain. Various mechanisms for pressure relaxation (diffusion) might be envisaged. As a model for pressure diffusion we might assume a one-parameter high-pass filter

$$p_w(\omega) = \frac{i\omega}{i\omega + q}\, p(\omega) \qquad (2\text{-}28)$$

where the pressure sensed in the well is related to aquifer pressure that is allowed to dissipate away if time is long enough. Alternatively we may assume all-pass behaviour

$$p_w(\omega) = \frac{i\omega + qr}{i\omega + q}\, p(\omega) \qquad (2\text{-}29)$$

if relaxation is incomplete. Which of the models is to be employed will depend upon the conditions that rule effectively at 14 days to 25 hours periods.

This is a very simple, heuristic approximation. The filters are not intended to represent drainage effects; for such situations the work of e.g. Rojstaczer should be consulted (e.g. Rojstaczer and Agnew, 1989). What this filter can provide is a crude constraint of causality. If residual phase lags are obtained after the fracture zone fit, the lag must be compatible with a change of response amplitude over frequency. See for instance Unbehauen (1971).

If we take the two lunar tides O_1 (diurnal) and M_2 (semidiurnal) the ratio of the pressure response Π_{M2}:Π_{O1} is a complex quantity which is relatively easy to obtain from the borehole record. Being a ratio it is independent of pressure efficiency factors at first order. Figure 2-8 shows the theoretical ratio based on the strain tides computed for KAS03 (including ocean loading strain) as a function of dip and azimuth of a fracture.

From Figure 2-8 can be seen that azimuth is relatively easy to resolve at all dip angles. At a particular value of the dip the response ratio has a singularity (M_2 respectively O_1 has a zero response, which is a consequence of the $E\beta$ term in equation (2-20); the dip range was therefore truncated in the figure.

The tidal stress-strain regime is horizontally controlled. We see that the M_2:O_1 response of steep fractures does not vary any more when dip gets close to 90 degrees. Therefore, to infer steep dip angles the absolute value of the response factor in the static-confined limit must be used, which depends on the elastic moduli of the geological formation.

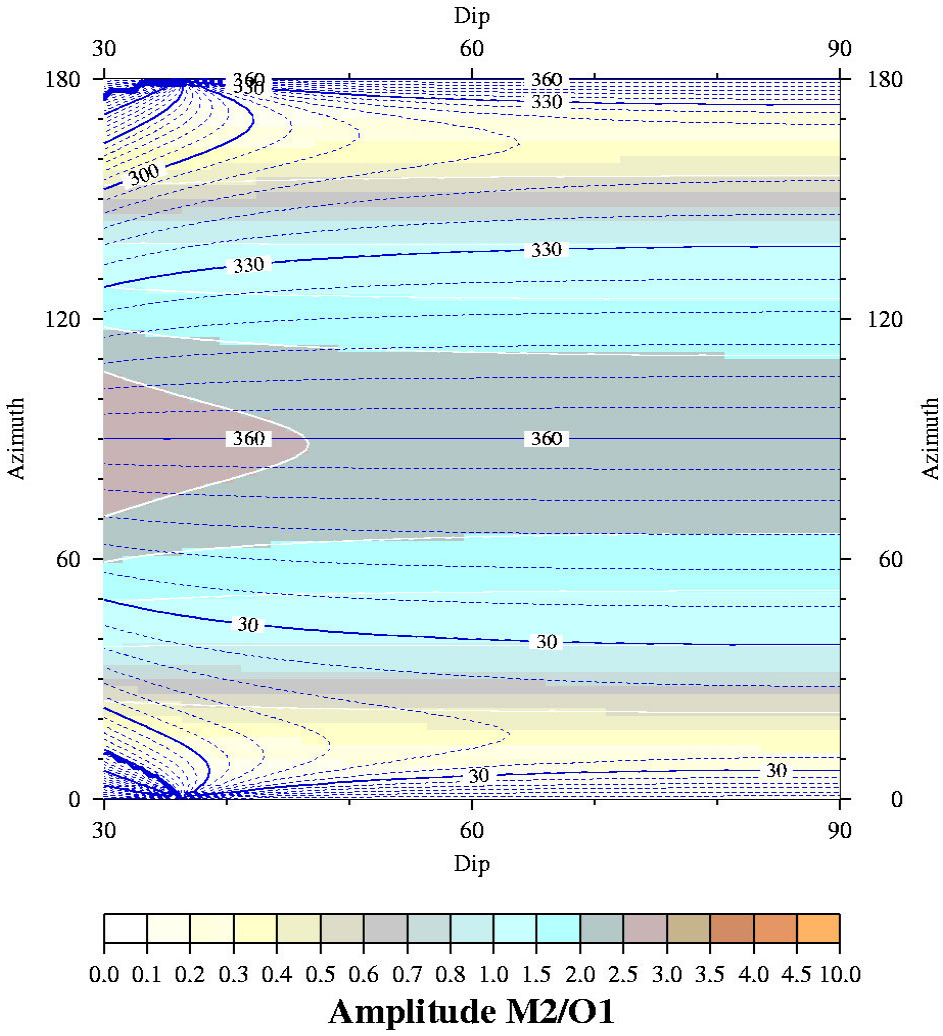

Figure 2-6. *Amplitudes (colours) and phases (blue lines) of the ratio of the tide response at the two most important lunar effects, O_1 (diurnal) and M_2 (semidiurnal) in the pressure in a packed section of a borehole. The ratio has been computed for strain tides at the KAS03 site (including ocean tide loading strain), and strain-pressure coupling has been computed for a fracture with varying dip (abscissa) and strike (ordinate) angles. The in-plane stretch ratio assumed is $E\beta$=20.*

2.3.2 The air pressure loading problem

Additional information may be added employing the barometric loading problem. The loading of air pressure implies instead a vertically controlled stress-strain regime. Under a loading slab of large but finite wavelength, areal strain approaches

$$\varepsilon_{zz} = \varepsilon_a \qquad (2\text{-}30)$$

(Farrell, 1972) which, using Rojstaczer and Agnew (1989), can be applied in the limiting case of an aquifer with negligible effect on the compressibility of the larger zone. So that

$$\sigma_{zz} = 2(\lambda + \mu)\varepsilon_{zz} \qquad (2\text{-}31)$$

$$\sigma_{nn} = \sigma_{ee} = (2\lambda + \mu)\varepsilon_{zz} \qquad (2\text{-}32)$$

and

$$\sigma_{ee} = \frac{1+2\nu}{2}\sigma_{zz} \qquad (2\text{-}33)$$

With this and $\sigma_{zz} = -p_a$ the Bower model can be extended with a barometric loading response.

$$\tau_n = (\sigma_{ee} + \sigma_{nn})x^2 + \sigma_{zz}z^2 \qquad (2\text{-}34)$$

$$\tau_t = (\sigma_{ee} + \sigma_{nn})z^2 + \sigma_{zz}x^2 \qquad (2\text{-}35)$$

where $z^2=\cos^2(D)$ and $x^2=\sin^2(D)$. Since the problem is uniaxial the relation between pressure in the fracture p_a and the barometric pressure p_b on the crust becomes rather simple,

$$p_a = p_b\left[\sin^2(D)\left(\frac{1+2\nu}{2} - \frac{1}{E\beta}\right) + \cos^2(D)\left(1 - \frac{1+2\nu}{2E\beta}\right)\right] \qquad (2\text{-}36)$$

Barometric efficiency expressed by the square bracket in (2-36) is shown in for a suite of Poisson ratios and a small set of different $E\beta$ parameters as a function of dip.

The barometric response is independent of the strike of the fracture zone. Modification of the pressure response could be accepted due to normal elastic aquifer behaviour. According to Van der Kamp and Gale (1983)

$$p = -\beta_c \frac{\sigma_{11} + \sigma_{22} + \sigma_{33}}{3} \qquad (2\text{-}37)$$

where β_c is the pressure fraction of the liquid in undrained and confined conditions,

$$\beta_c = \left(\frac{1}{K} - \frac{1}{K_s}\right)\left[\frac{1}{K} - \frac{1}{K_s} + n\left(\frac{1}{K_f} - \frac{1}{K_s}\right)\right]^{-1} \qquad (2\text{-}38)$$

the incompressibilities are denoted as follows, K - aquifer, K_s - rock matrix, and K_f - fluid; n is the porosity.

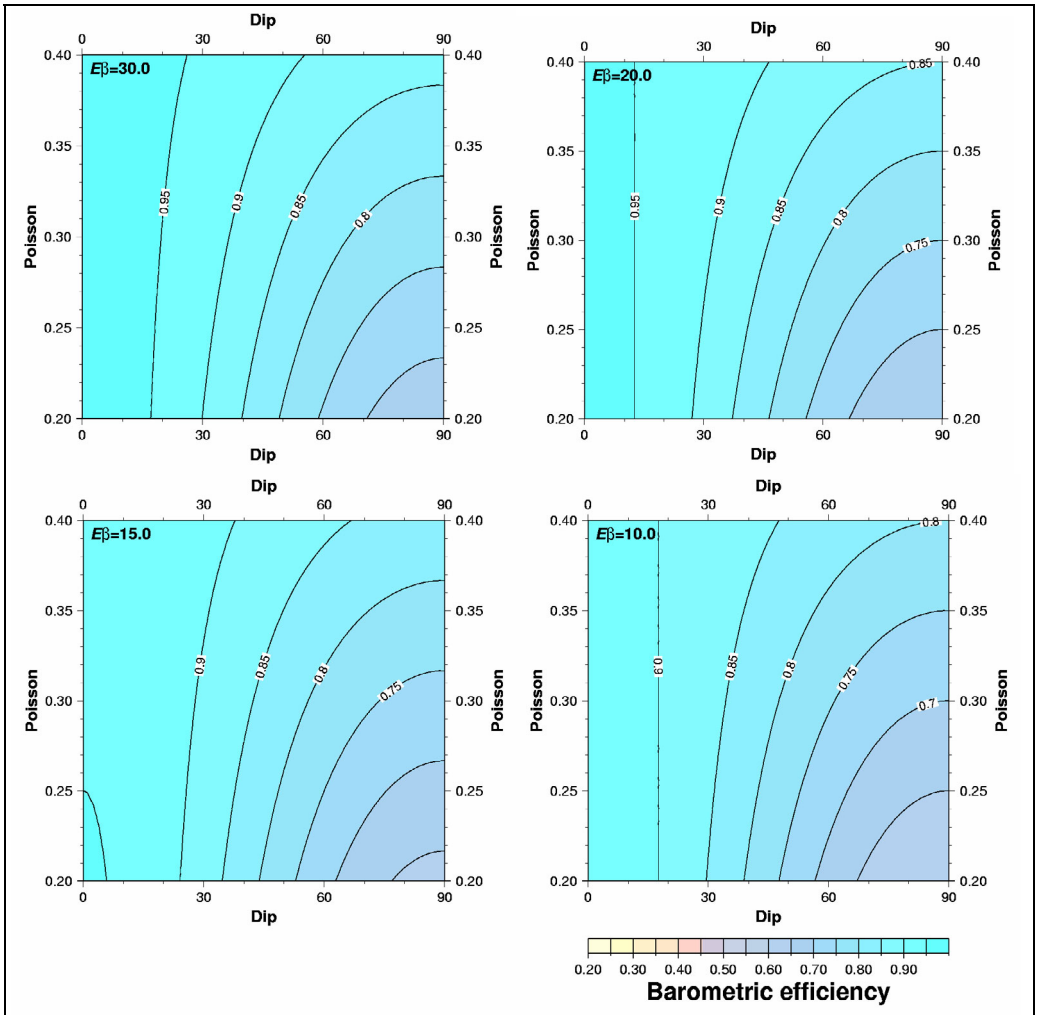

Figure 2-7. *Barometric efficiency in a fracture, varying dip angle and Poisson's ratio. Each frame is for a specific value of the in-plane fracture stretch quotient Eβ.*

2.3.3 Estimation of fracture zone parameters

The following parameters determine the fracture zone response:

- D and A (dip and azimuth angles)
- λ, ν, $E\beta$ (rock parameters)
- q (pressure diffusion model)
- q_{eff} or q_x (strain-pressure transmission efficiencies)

Of course, $\mu = \dfrac{1-2\nu}{2\nu}\lambda$.

For the tidal problem we have as input variables the strain components

$$\varepsilon_{ee}, \varepsilon_{nn}, \varepsilon_{ne}$$

This would be a time-domain formulation. In the frequency domain the tides are specified in the form of complex valued coefficients relating to the phase of the astronomical tide potential, equation (2-4). The output (pressure) is related to the input (strain components) through

$$\tilde{\Pi}_k = \frac{i\omega_k}{q + i\omega_k} \sum_{rs} F_{rs}(A, D, \lambda, \nu, E\beta)\, \tilde{\mathrm{E}}_{rs,k} \qquad (2\text{-}39)$$

where the function F_{rs} is obtained from substitution of equations (2-17) into (2-12) and (2-13), from there into (2-11). At last, multiplying with the dispersion function (2-20) or (2-21) by which Π_k is predicted.

The dispersion parameter q can be determined in a separate step in which only the three strain coupling parameters β_1, β_2, β_3 are solved (cf equation 2-14, a linear problem).

The task is now to find a set of parameters that minimises the prediction error. Since many of the parameters have a nonlinear influence a Levenberg- Marquardt algorithm (Press et al., 1992, Chap. 15.5) can be employed. The partial derivatives $\frac{\partial F_{rs}(\xi_j)}{\partial \xi_j}$ are needed. They are straightforward to derive, but are omitted here for reason of space.

The problem turns out to be slightly ill-posed at steep dip angles. There D and λ are found to have high covariance and thus cannot be determined independently. This is so since at steep dip angles the $E\beta$ term makes only small contributions; thus $E\beta$ cannot be well-determined either. Adding tide observations in the diurnal and semidiurnal bands enters unique information mostly because ocean loading strain injects a certain range of ratios between strain components in the same band, but these are small signals only. Similarly the long-period tides add new combinations of strain components, but come with only small signal strength. The range of permissible values for Poisson number ν is quite narrow. It also has covariance problems with λ and D. Thus, the key parameters to solve are A, and D and one more parameter while the others are kept at known or uncritical a priori values.

The trade-off between λ and D is basically described by the relation

$$\lambda \cos^2 D = const \qquad (2\text{-}40)$$

i.e.

$$\frac{d\lambda}{dD} = -2 \tan D$$

Thus it appears highly desirable to know λ from independent sources in the case of steeply dipping fractures. The immediate possibility is to use seismic P- and S-wave velocities and rock density, and compute

$$\lambda = \rho(v_p^2 - 2v_s^2)$$

2.4 Signal processing

2.4.1 Noise whitening

Linear least-squares estimation supposes that a signal is estimated in incorrelated noise, alternatively that an operator is defined that describes the covariance between errors in observed data.

$$\mathbf{Ax} = \mathbf{d}\,, \quad (\mathbf{d} - \mathbf{Ax})^T \mathbf{W}^{-1} (\mathbf{d} - \mathbf{Ax}) \stackrel{!}{=} \min$$

has the inverse solution

$$\mathbf{x} = (\mathbf{A}^T \mathbf{W}^{-1} \mathbf{A})^{-1} \mathbf{A}^T \mathbf{W}^{-1} \mathbf{d}$$

Alternatively, and—as we shall see—suitable in the case of time-series

$$\mathbf{A'x} = \mathbf{d'}\,, \quad (\mathbf{d'} - \mathbf{A'x})^T (\mathbf{d'} - \mathbf{A'x}) = \min$$

$$\mathbf{x} = (\mathbf{A'}^T \mathbf{A'})^{-1} \mathbf{A'}^T \mathbf{d'}$$

with

$$\mathbf{A'} = \mathbf{W}^{-½} \mathbf{A} \quad \text{and} \quad \mathbf{d'} = \mathbf{W}^{-½} \mathbf{d}$$

The latter task is seen as data noise whitening. It can be carried out using a predicition error filter. In order to preserve the degrees of freedom of the original problem, the filter is determined on the following special residual time series

$$\mathbf{r} = \mathbf{d} - \mathbf{Ax} + \mathbf{A}\eta$$

where η_n is normally distributed according to N(0,σ_{xn}).

A suitable algorithm for the noise whitening procedure has been given by Burg (1972). See also Claerbout (1976, Chap. 7)

2.4.2 Wiener filtering

If we describe an input-output relation of a linear system as

$$y = h * x + \delta = u + \delta$$

then h is called a Wiener filter if it predicts a known output y from x while δ is uncorrelated noise. Realisations of the filter h can be based on cross-spectral estimation, using the complex admittance spectrum and the coherence spectrum. Denoting all variables in the frequency domain by the associated upper-case characters, we have

$$H(f) = \frac{|U(f)|^2}{|U(f)|^2 + |\Delta(f)|^2}$$

(c.f. Press et al., 1992, Chap.13.3) This can be approximated by

$$H(f) = \frac{YX^*(f)\mathrm{K}^2(f)}{|X(f)|^2}$$

where $\mathrm{K}^2(f)$ is the squared coherency spectrum

$$\mathrm{K}(f) = \frac{|YX^*(f)|}{|X|^2(f) + |Y|^2(f)}$$

and the cross-spectra and power spectra are computed from windowed estimates of auto- and cross-covariance, respectively, by Fourier transformation

$$YX^*(f) = \mathrm{s}_s\{\mathrm{E}[y_t x_{t+\tau}]\}$$

In the estimator there is a window involved. Also, before the spectrum operations can be performed, the input signal x needs to be whitened and the same filter needs to be applied on the signal y in order to fulfil the requirements for least-square adjustment (which this analysis is implicitly based on). This tampering needs to take into consideration over which time-scales correlation between input and output could still be possible.

The resulting filter is then produced with a windowed version of the inverse transformation in order to yield a conveniently short series,

$$h_\tau = \text{☞}^{-1}\{H(f)\} w_\tau$$

Thus, the Wiener filter is a windowed version of the inverse of the admittance spectrum weighted by the squared coherence spectrum.

Wiener filtering is used in the data analysis in order to remove the stochastic component that correlates with air pressure or other types of perturbations acting on the well pressure. If this influence were instantaneous, a step in the excitation yielding a step in the well pressure with no delay and no decay, a single admittance coefficient would suffice.

3 Experience from analysis of KAS03 borehole records

3.1 Description of the records

Figure 3-1 shows the data records that were analysed together. The KAS03 **borehole pressure** time series covers the time period between July 10 and December 6, 1989. It is sampled in units of water head at approximately 1 mm resolution and one hour intervals. This series has been made available from Geosigma Uppsala.

In addition I have acquired **air pressure data and sea level data** measured at Ölands Norra Udde from SMHI. Also, air pressure data from Västervik was obtained. The air pressure series is sampled at three hours interval and 0.1 hPa resolution. The tide gauge data is sampled at one hour interval and 1 cm resolution.

Results from an analysis for solid-earth tide related problems obtained from this time series was recently presented at the International Earth Tides Symposium (Scherneck, 2001).

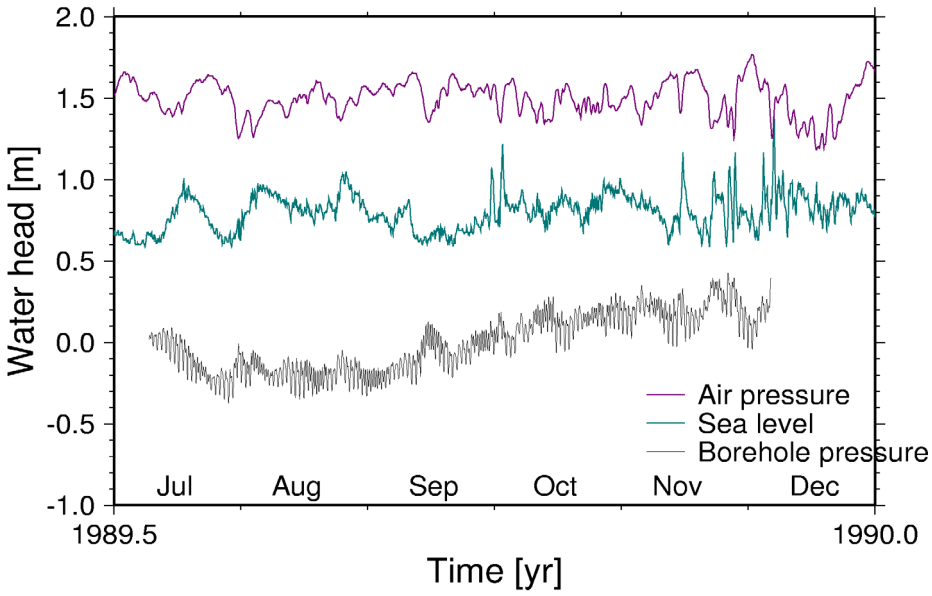

Figure 3-1. *Observed time series. Sampling interval of the borehole pressure and the sea level is 1h, air pressure 3h. The latter two were acquired from SMHI.*

3.2 Data analysis

An overview of existing software is given in Section 4 together with a flowchart (Fig. 4-1). The following sections will detail how the results of tidal and barometric analysis of the KAS03 borehole record were obtained using the theoretical basis developed in Section 1.

3.2.1 Tide analysis

The duration of the time series, 149 days, permits spectral resolution at half-year periods at maximum. The following tide bands were analysed, where wave group membership is decided by identical argument numbers in the emphasised fields

The program computes complex admittance coefficients between each band and the observed time series (the coefficients $\tilde{\Pi}_j$ in equation (2-10)). The band (wave-group) signals represent the tide gravity potential (units are $m^2 s^{-2}$). For convenience we divide by g (mean gravity acceleration, 9.81 $m s^{-2}$; the admittance coefficients for water head are then dimensionless numbers).

Since the process of fit is based on least squares, the temporal correlation of the data must be reduced. This is done using a short prediction error filter, computed with Burg's Maximum Entropy method (Claerbout, 1976). All signals involved in the fitting process are filtered. Before that, DC signal components are removed. Missing data points are not interpolated. The filtering will have the unfortunate side effect to add its length to the length of each gap in the input series. The fact that MEM filters will be as short as possible helps to cope with the gap problem, however.

The fitting process is rerun three times. First, the air pressure series is used as an additional signal for fit, estimating one real-valued coefficient. The first series of complex tide coefficients is used to compute a first forward prediction. The tide-residual (observations minus predicted tides) is then used to construct a Wiener filter (Press et al., 1992, Chapt. 13.3) for air pressure.

Table 3-1. Tide wavegroups analysed

	τ	s	h	p	N	p_s	π/2	freq [cyc/d]	Lunar Solar	
M_m	0	1	0	-1	0	0	0	0.03629	L	monthly, elliptical
M_f	0	2	0	0	0	0	0	0.07320	L	semi-monthly, declin.
M_t	0	3	0	-1	0	0	0	0.10949	L	ter-monthly, elliptical
σ_1	1	-3	2	0	0	0	-1	0.86181	L	diurnal, variational
Q_1	1	-2	0	1	0	0	-1	0.89324	L	diurnal, elliptical
O_1	1	-1	0	0	0	0	-1	0.92954	L	diurnal, declinational
M_1	1	0	0	1	0	0	1	0.96645	L	diurnal, elliptical
P_1	1	1	< -1	0	0	0	-1	0.99726	S	diurnal, declinational
K_1	1	1	≥ -1	0	0	0	1	1.00274	LS	diurnal, declinational
J_1	1	2	0	-1	0	0	1	1.03903	L	diurnal, elliptical
ω_1	1	3	0	0	0	0	1	1.07594	L	diurnal, declinational
$3N_2$	2	-3	2	1	0	0	0	1.82896	L	semi-d., elliptical
$2N_2$	2	-2	2	0	0	0	0	1.86455	L	semi-d., elliptical
N_2	2	-1	0	1	0	0	0	1.89598	L	semi-d., elliptical
M_2	2	0	0	0	0	0	0	1.93227	L	semi-d., pricipal
L_2	2	1	0	-1	0	0	2	1.96857	L	semi-d., elliptical
S_2	2	2	-2	0	0	0	0	2.00000	S	semi-d., pricipal
K_2	2	3	0	-1	0	0	0	2.04177	LS	semi-d., declinational
3-1	1	0	0	0	0	0	2	0.96614	L	n=3, diurnal
3-2	2	-1	0	0	0	0	1	1.89567	L	n=3, semi-diurnal
M_3	3	3	0	0	0	0	2	2.89841	L	n=3, ter-diurnal

In the second rerun the Wiener-predicted air pressure is used instead of the direct pressure variation. With this setting a new set of tide parameters is computed, and a new Wiener filter for air pressure is computed.

In the third round the tide gauge time series is included in the signal model. Also, the n=3 tides are predicted and subtracted from the input in order to keep the number of estimated parameters small and limit them to large effects only.

> Actually, the tides with n=3 are predicted using the strain coupling model that is determined from the n=2 tides. An advantage of forward modelling these tides is to avoid aliasing of n=2 tides into the n=3 tide band, i.e. biasing of admittance coefficients.

Now, one could go about the same way with the tide gauge record as with air pressure, i.e. estimate a Wiener filter. However, the influence of the water level on the borehole pressure turns out as being relatively small, so the iteration may stop here.

The results for the eight most important tides are shown in Table 3-1. The admittance coefficients have been multiplied with the potential amplitudes to reproduce the cosine amplitude in units of millimetre of the water head in the borehole section.

The residual of the third iteration, observations minus predicted using all estimated coefficients, is shown in Figure 3-3. A zoom into a 720 h long section of the residual record is also shown.

Table 3-2. Results of tide analysis.

Tide or time series	Potential amp. [mm]	Amplitude [mm], phase [°] in iterations 1	2	3
M_f	23.5	6.2±5, 175°	4.3±5, 182°	2.5±4, 176°
Q_1	17.6	6.5±1, 220°	6.1±0.6, 217°	6.3±0.5, 217°
O_1	91.5	33.8±0.5, 211°	33.6±0.5, 211°	33.7±0.5, 211°
P_1	39.4	14.7±0.5, 208°	14.7±0.5, 207°	15.2±0.5, 208°
K_1	94.5	38.2±0.5, 210°	38.0±0.5, 210°	37.8±0.5, 209°
N_2	13.6	8.5±0.6, 206°	8.6±0.6, 206°	7.8±0.3, 206°
M_2	70.9	41.8±0.3, 204°	41.9±0.3, 204°	41.7±0.3, 204°
L_2	2.0	1.1±0.3, 203°	1.4±0.3, 230°	1.1±0.3, 203°
S_2	33.0	19.8±0.2, 205°	20.2±0.2, 203°	20.1±0.2, 203°
M_3	0.05	0.2±0.2, 204°	0.2±0.2, 209°	n.e.
air press.	-	-0.483±0.013 [1])	n.e.	n.e.
air p (WF)	-	n.e.	1.32±0.3 [2])	1.34±0.3 [2])
water level	-	n.e.	n.e.	0.084±0.5 [3])

WF Predicted air pressure effect on aquifer using a Wiener-filter
n.e. not estimated
[1]) admittance, water head due to air pressure, [mWH/hPa]
[2]) dimensionless admittance, [-]
[3]) admittance, water head due to sea level, [mWH/m]

A last variant treats air pressure influence in a two-route fashion. The concept is that air pressure variations with solar sinusoidal cycles are not necessarily admitted into the borehole pressure with the same quantitative relation as the nontidal part. Nontidal in this context means the variations generated by solar radiation. These consist of one, two and three cycle per year and one and two cycles per solar day. The solar-excited cycles could for instance have much better spatial coherence, and thus load the crust more efficiently. But also, they might be found in the borehole signal because of effects of other origins that happen to have solar cycles.

The tide part of the air pressure signal can be discriminated using the solar radiation tide spectrum given in Cartwright and Tayler (1971).

Thus, if the air pressure signal is split into a tide-free part, which again is passed through a Wiener filter, and a separate tide part, the tide response and air pressure admittance figures change slightly for the waves P1, K1, L2 and S2.

3.2.2 Strain coupling parameters

When the tide admittance coefficients are available, strain coupling coefficients are estimated from a least-square fit of predicted strain tide coefficients, including ocean loading effects, against the observed pressure admittance coefficients, cf. equation (2-13). The only nonlinear parameters involved in this fit are the parameters in the term $Q(i\omega)$ accounting for dissipation, cf. equation

Table 3-3, Table 3-2 continued. Iteration number 4, air pressure along two routes of admittance (indirectly through sea level and direct).

Tide or time series	Potential amp. [mm]	Amplitude [mm], phase [°] in iteration 4
M_f	23.5	2.6±4, 226°
Q_1	17.6	6.3±0.5, 210°
O_1	91.5	33.7±0.5, 210°
P_1	39.4	15.8±0.5, 207°
K_1	94.5	38.4±0.5, 209°
N_2	13.6	7.8±0.3, 205°
M_2	70.9	41.7±0.3, 204°
L_2	2.0	1.1±0.3, 202°
S_2	33.0	21.1±0.9, 200°
air p (SRF)	-	0.85 ±0.4 [1])
air p (WF)	-	1.341±0.033 [1])
water level	-	0.085±0.005 [2])

WF Predicted air pressure, Wiener-filter and SRF notch filter
SRF Solar radiation filter
n.e. not estimated
[1]) dimensionless admittance, [-]
[2]) admittance, water head due to sea level, [mWH/m]

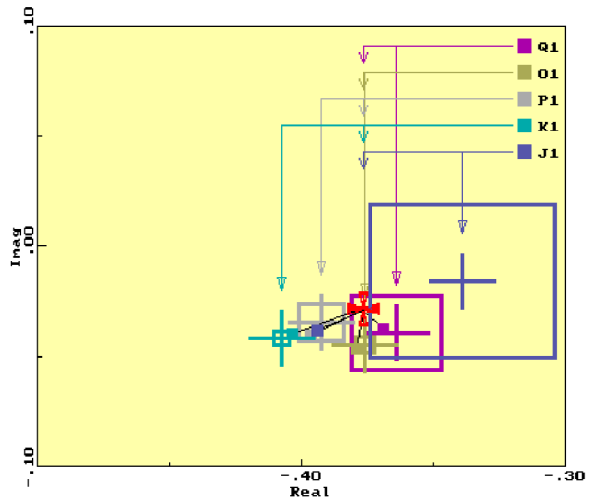

Figure 3-2a. *Diurnal tide phasors. Complex admittance coefficients are shown. Solid earth tide is indicated by the red Maltese cross; this parameter has become constant throughout the diurnal frequency band after the liquid earth core resonance has been filtered out. The small solid rectangles represent the additional ocean loading strain. The observed admittances are indicated by crosses surrounded by rectangles with the size of the 95% confidence interval.*

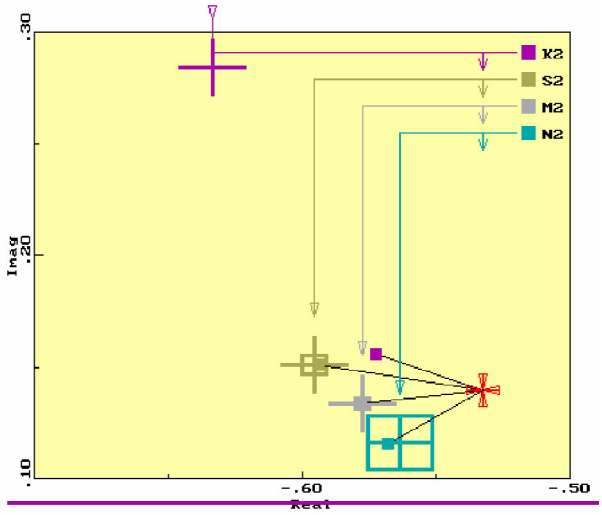

Figure 3-2b. *Semidiurnal tide phasors. The solid earth tide phasor is displaced from the real axis as a unique consequence of coupling of north-east strain. K_2 is only a small tide effect; the detection confidence limit is wider than the plotting frame (it shows as a purple bar along the bottom)*

(2-28) or (2-29). The actually used model here is

$$Q(i\omega) = \frac{i\omega + qr}{i\omega + q}$$

where r is the "relaxed response" ($\omega \to 0$) and $2\pi/q$ is a relaxation time.

The problem is solved with the Levenberg-Marquardt algorithm. The tide admittances are restored to their **static-confined** estimates by multiplying them with Q^{-1}. Typical values found in KAS03 are r=0.61±0.015 and $2\pi/q$=72±4 hours. The fit is indicative of how uniformly with respect to frequency the observations can be reconciled with a constant set of coupling coefficients, three real-valued parameters. The χ^2 of fitting 22 tide parameters (11 complex values) is found to be 23, which is almost as perfect as it can get. See Figure 3-2 for illustration.

3.2.3 Fracture zone parameters

Solving for the fracture zone parameters equation (2-29) is turned into an observation equation. Thus, the problem is attacked on the stage of tide admittance.

The observed well pressure amplitudes and phases are recast into real and imaginary parts. The χ^2 measure of fit is set up as the sum of squares of the model misfit, dividing by the squared uncertainty of each observation.

Table 3-4. Solution for fracture zone parameters

	Solution 1	Solution 2
Dip	$83^o \pm 40^o$	$74^o \pm 3^o$
Azimuth	$123.2^o \pm 0.3^o$	$123.0^o \pm 0.3^o$
Poisson	0.27 fixed	0.294 ±0.02
Lamé λ	25 ±7 GPa	30 GPa fixed

The tide synthesis formulas for strain, (2-1), (2-3), (2-4) and (2-7), ocean loading effects added from equation (2-17), are used to compute the predicted tide at the measurement epoch. The corresponding phase-quadrature signal is computed simultaneously (using complex exponential instead of cosine in equation (2-3)). By this we establish amplitude and phase relations between the local tide strain components and the tide potential at the epoch of the experiment.

The dispersion of the observed coefficients (imaginary parts, differences between diurnal and semidiurnal amplitudes are the primary effect of strain coupling. The dispersive prefactor accounts for a few degrees of phase shift and a few percent in amplitude variation between the diurnal and semidiurnal bands. The efficient contributor to the out-of-phase component of the well pressure is the north-east component of strain; the efficient modifier between the diurnal and semidiurnal gain (amplitude of admittance) is the difference between east and north strain.

Finally the tide parameters are analysed with respect to fracture zone parameters. I show two solutions, one where λ has been solved and ν has been fixed at 0.27, and one where λ has been fixed at 30 GPa and ν has been solved.

See the discussion in section 2.3.3. We find that holding the Lamé modulus fixed at a value determined from e.g. seismic surveys is preferable. The large covariance of Dip with with λ is avoided. The fracture zone dip will then largely depend on seismic results and density. Azimuth is always very well resolved, and a reasonable value for the Poisson parameter is also obtained.

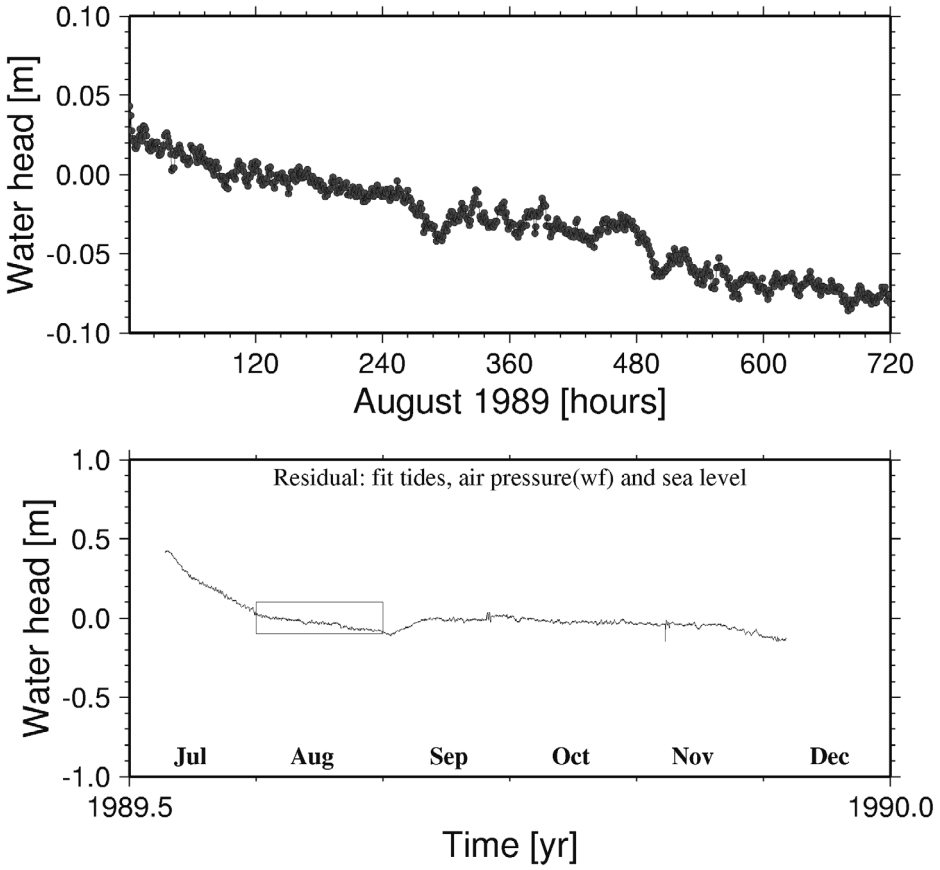

Figure 3-3. *The residual after removing predicted tides, air pressure and water level effects using a least-squares fit. Top frame blows up the rectangle of the lower frame.*

3.2.4 Air pressure effects

Figure 3-1 showed the barometer time series recorded at Ölands Norra Udde by SMHI. The time series is originally sampled at 3 h interval. For the following cross-spectrum analysis I have interpolated the time series to line up with the borehole data. This is to be kept in mind when looking at the spectrum above the original Nyquist frequency, 4 cyc/d. The time series are shown again in Figure 3-4.

The causality of the system is easily analysed. Air pressure is treated as an input, aquifer behaviour as the transfer system, and borehole pressure as the output. To estimate the transfer spectrum, the spectrum of **barometric efficiency,** the time series is filtered by a prediction-error filter in order to yield white noise at the output. For the borehole pressure the residual of the simple tide analysis is used, i.e. the series where no attempt has been made to reduce air pressure effects. This series is also filtered with the same whitening filter.

The cross-spectrum estimation employed in the following uses the Bartlett method for autocovariance and cross-covariance estimation (Oppenheim and Shafer, 1975, Chap.11) and provides coherence, gain, and phase spectra that are computed from these series. Confidence limits are computed following Jenkins and Watts (1968, Chap.10).

The spectra for coherence, gain and phase are shown in Figure 3-5, Figure 3-6, and Figure 3-7. Well pressure and barometric pressure are highly correlated at low frequencies, significant coherence persisting to slightly above 1 cycle per day. The barometric admittance appears to be quite stable below 1 cyc/d with at most 30 degrees phase lag with respect to an inverted barometer response. Using the same pressure units for aquifer and air, the barometric gain is a dimensionless number, estimated at

- gain = -0.52±0.02 (air pressure acting on rock unit and water head)

The aquifer-only gain factor, the **barometric efficiency proper** (BEP), is obtained by adding unity to this value, i.e.

- BEP = 0.48±0.02 (air pressure acting only on rock unit)

It would be interesting to study the high-frequency branch of the gain curve more closely, but in this part of the air pressure spectrum, the geographical distance of 20 km between Äspö and Ölands Norra Udde might incur problems and misinterpretation. The departure of the phase curve from the 180 degree level might also relate to the site separation, and to the fact that synoptic pressure systems and weather fronts do have preferred directions of motion.

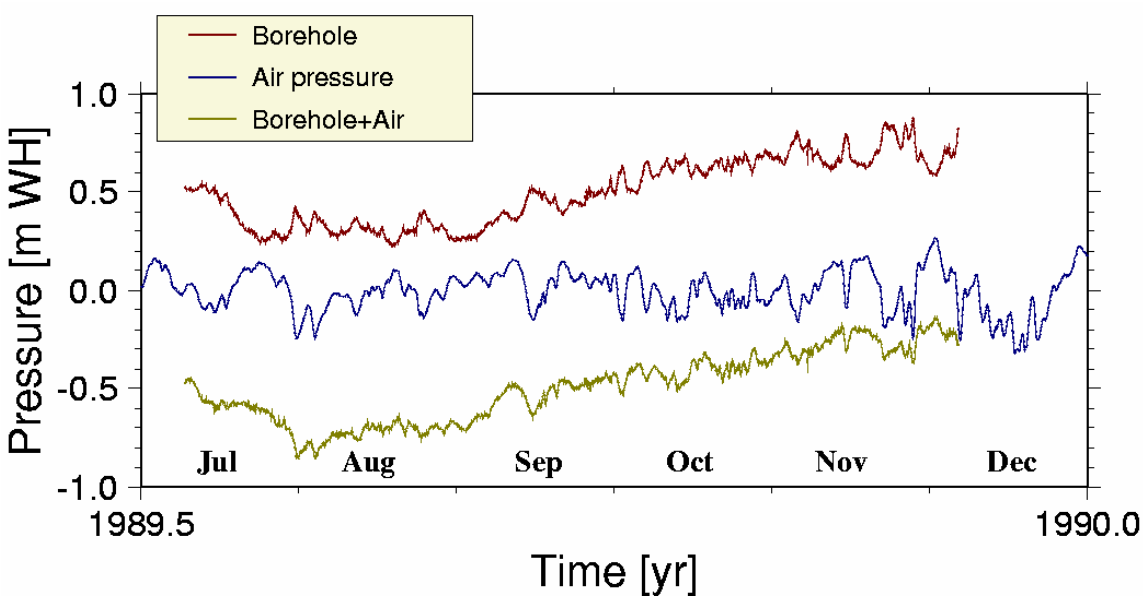

Figure 3-4. *Tide residual of borehole record (red), air pressure from Ölands Norra Udde (blue), and the sum of both (grey) as a proxy for aquifer pressure in absence of a borehole.*

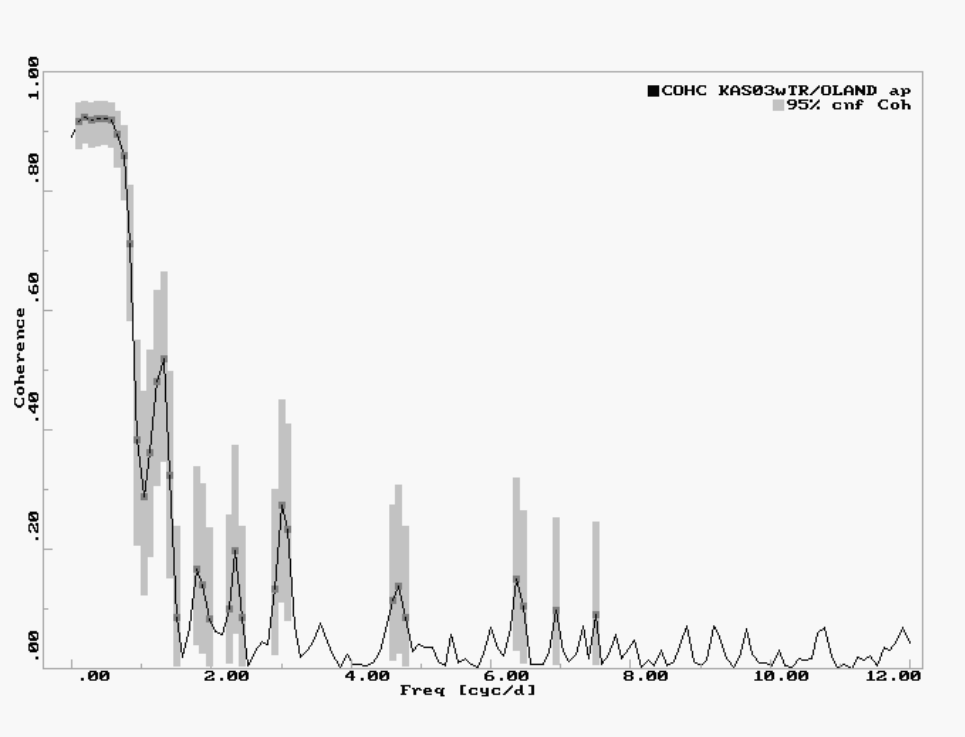

Figure 3-5. *Coherence between barometric pressure at Ölands Norra Udde and well pressure in KAS03. Green bars indicate 95% significance; where missing coherence is insignificant.*

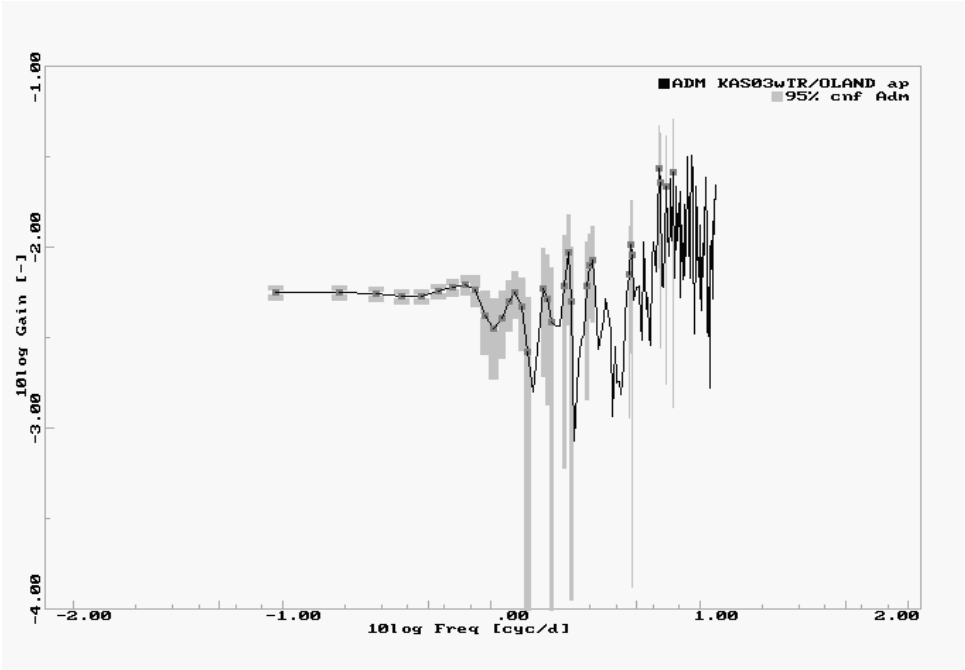

Figure 3-6. *Gain spectrum of borehole pressure with respect to barometric pressure. Borehole pressure is measured relative to ambient pressure and given in units of meter equivalent water head. Barometric pressure is measured 20 km away at Ölands Norra Udde and given in units of hectopascal. Both axes are logarithmic. The logarithm of gain were -2 if the aquifer had no response at all.*

3.3 Discussion and interpretation of results

The tide and barometric results from the KAS03 analysis are now put together and discussed. The gain and phase spectra of the barometric analysis suggest that the dominating effect is the direct effect of air pressure on the back end of the pressure measurement device. This corresponds to depressing the well head in an infinitely narrow borehole. Corrected for this effect, the barometric efficiency estimated is surprisingly low, near 0.5. Such a low value could only be reconciled with small voids and balanced aspect ratios (i.e. small values of $E\beta$), extremely small values of the Poisson ratio and very steep fractures.

An additional, fracture related efficiency factor might have to be introduced. For the relatively low value of Poisson, 0.25, a 90 degree dip, and $E\beta$=10 this factor would have to be as low as 0.7. To some part the low magnitude could be explained by the Baltic Sea yielding to air pressure and decreasing the load on the crust; however, these processes work well only at periods of several days and longer. Particularly in a shallow, almost enclosed basin the barometric equilibrium is even more time-delayed. Probably, the fracture (-system) is open only to a smaller extent, while wall-to-wall contacts take up much of the stress.

If one assumes the efficiency parameter to represent the transmission of stress in the rock to the fluid, then it should apply in the tide problem in exactly the same way.

From the tide results the amplitudes are given by Lamé modulus λ, found in the range of 25±7 GPa and an attenuation factor (accounting for "dispersive effects") that deviates from unity negligibly. Also the tide results hint at a very steep fracture zone. If the observed tide response is attenuated with 0.7, the actual λ is more close to 25/0.7=36 GPa, which means a compressive seismic wave velocity v_p=6300 ms^{-1}.This value is somewhat high, but basically compatible with the Nafe and Drake velocity curve for igneous rocks of type diorite or granite (see Fowler, 1990, p.79).

These results might still have to be taken as preliminary because air pressure measurements from the site would be preferable. The barometric loading analysis can then be modified to work with the inferred aquifer pressure

A simultaneous inversion of fracture zone parameters from both tides and barometric loading results is desirable. This is proposed for the next stage of the analysis (only a few lines of computer code need to be changed).

In our case the prefactor designed to absorb wide-band low-pass or high-pass behaviour (assuming pressure dissipation into weakly connected void systems) showed only little frequency structure. This is compatible with the almost constant barometric efficiency over a wide range of sub-diurnal frequencies. In general however, there lies a risk within here, that parameters might be misidentified. The wide-band response of both tides and barometric pressure is needed to assure that pressure dissipation is low, or to provide the observations necessary for designing a transfer model for the dissipative effects. This means that long-period tides need to be resolved. In KAS03 we find the fortnightly (M_f) tide at an amplitude between 2 and 6 mm with an error of 4 mm. The determination of M_f depends on long data series, high measurement resolution and low noise conditions.

The problem with the need of long-period information to secure the quality of the aquifer parameter solution (particularly to avoid systematic errors in the fracture zone strike angle, which is determined with low formal stochastic errors) could possibly be reduced by having barometric data from the site at high quality.

In any case, it appears necessary to analyse at least several weeks worth of data in order to resolve the behaviour of the fracture down to frequencies of 0.1 cycles per day (stacking factor 4 for power spectral analysis times 20 days equals 80 days.

It is yet proposed to try and gain experience from shorter time series and compare fracture zone parameters with observed ones using a simple barometric and dissipative response model. An efficiency factor for the fracture can be obtained from barometric analysis from probably one to two weeks of data (except in situations of stationary weather systems), which can provide the factor that largely controls the fracture dip estimate.

3.4 Conclusions

Hourly sampled data of well pressure obtained between packers at a 720 m deep section of the KAS03 borehole on Äspö was used in a tide and barometric response analysis. Air pressure and sea level data from Ölands Norra Udde, approximately 20 km to the east of Äspö, was used as ancillary data. In the tide analysis the air pressure-induced response was modelled by Wiener filtering in order to reduce the systematic influence in the borehole record. The Wiener filtered barometric record and the series from the sea level of the Baltic Sea were than fitted to the observations. It turned out that also the sea level in the neighbourhood has a significant influence on the borehole pressure.

The barometric analysis also provided a parameter for barometric efficiency. It turns out to be quite constant at frequencies between 0.1 to 2 cycles per day. A slight phase lag towards the high frequency end of the spectrum could be related to the fact that the pressure is measured at the 20 km distance mentioned above. The low value for the inferred aquifer-only barometric efficiency calls for assuming a stress transmission coefficient. The efficiency found is as low as 0.5. It may be interpreted as the fractures being open only for a limited fraction of the surface area.

The dominating signals found in the pressure record are due to solid earth tides and global ocean loading effects. It is obviously the tidal strain which controls borehole pressure. Using a fracture zone model one can explain the pressure variation with a set of parameters for the strike and the dip of the fracture zone.

The parameter for the strike angle of the fracture is almost always resolved with very low uncertainty. This quantity is quite safe to estimate. It can become biased only if the amplitude ratios of the response in the tide bands cannot be reconciled with the strain coupling model; then the phase of the response would be offset by resorting to a strongly frequency-dependent factor for diffusion or pressure relaxation.

A mixture of effects from normal aquifer behaviour (depending only on areal strain but showing a lot of frequency structure in the response at intermediate periods) and a fracture zone with fluid-filled cracks (showing frequency dependence due to coupling of deviatoric tidal strain) can make the problem more difficult. There is a trade-off between parameters characterising the frequency-dependence in both cases.

The measurement method employed by Geosigma has the advantage that it avoids drainage to the well. A as logical disadvantage, transmissivity and storativity parameters cannot be addressed.

The suggested strategy to solve fracture zone parameters is as follows. Elastic parameters for the larger geological unit (λ and ν) are derived from seismic profiles and from rock density. The remaining parameters to be estimated are the stress transmission efficiency, strike, and dip. The three parameters can only be solved with the necessary redundancy if tides and barometric efficiency are analysed jointly.

4 References

Aki K, Richards P G, 1980; *Quantitative Seismology, Theory and Methods, Volume II.* Freeman, San Francisco, pp. 559-935.

Annor A, Geller L, 1978; Dilatational velocity, Young's modulus, Poisson's ratio, and uniaxial compressive strength for CR6 samples, *Techn. Data 303410-M04/78,* Can. Centre for Miner, and Energy Technol., Ottawa, Ont. (not seen; ref. in Bower, 1983).

Arfken G, 1985; *Mathematical Methods for Physicists.* Academic Press, San Diego, Cal., 3rd edition, 985 pp.; cf R 5.7-1

Biot M A, 1941; General theory of three-dimensional consolidation. *J. appl. Phys,* **12,** 155-164.

Bower D R, 1983; Bedrock fracture parameters from the interpretation of well tides, *J. Geophys. Res.,* **88,** 5025-5035; cf R 3.4-2

Bredehoeft J D, 1967; Response of well-aquifer systems to earth tides. *J. Geophys. Res.,* **72,** 3075-3087; cf R 5.3-3

Burg J P, 1972; The relationship between maximum entropy spectra and maximum likelihood spectra. *Geophysics,* **37,** 375-376.

Büllesfeld F-J, 1985; *Ein Beitrag zur harmonischen Darstellung des gezeitenerzeugenden Potentials.* Deutsche Geodätische Kommission, Reihe C, Dissertationen, Heft Nr. 314, Verlag Bayerische Akademie der Wissenschaften, München, 103pp.

Cartwright D E, Tayler R J, 1971; New computations of the tide-generating potential. *Geophys. J. R. Astron. Soc.,* **23,** 45-74; cf R 5.2-4

Claerbout J F, 1976; *Fundamentals of Geophysical Data Processing,* McGraw-Hill, 274 pp.; cf R 5.7-5

De Vries J J, Gieske A 1988; Barometric tides in partly-saturated confined aquifers in Botswana. *J. Hydrology,* **104**, 17-32; cf R 5.4-6

Delcourt-Honorez M, 1986; Earth tide response and barometric effect in three well-aquifer system; the effect on gravity of the three waterlevel variations. In Vieira R (ed): *Proceedings 10'th Int. Symp. Earth Tides,* pp 843-854. Consejo Superior de Investigaciones Cientificas, Madrid; cf R 5.6-7

Delcourt-Honorez M, 1991; Water level fluctuations in a borehole at the Royal Observatory of Belgium: Effects on local gravity, earth tides and barometric responses. In Kakkuri J (ed): *Proceedings 11'th Int. Symp. Earth Tides,* pp 389-412, Schweizerbart'sche Verlagsbuchhandlung, Stuttgart; cf R 5.6-8

Endom J, Kümpel H-J, 1994; Analysis of natural well level fluctuations in the KTB-Vorbohrung - Poroelastic aquifer parameters and single fracture models. *Scientific Drilling*, **4**, 147-162; cf R 5.3-9

Farrell W E, 1972; Deformation of the earth by surface loads, *Rev. Geophys. Space Phys.,* **10,** 761-797; cf R 5.2-10

Fowler C M R, 1990; The Solid Earth. An Introduction to Global Geophysics. Cambridge University Press, Cambridge, U.K., 472pp.

Gilbert F, Dziewonski A, 1975; An application of normal mode theory to the retrieval of structural parameters and source mechanisms from seismic spectra, *Phil. Trans. R. Soc.,* **278A,** 187-269.

Hanson J M, Owen L B, 1982; Fracture orientation analysis by the solid earth tidal strain method. In: *Proc. 57'th Annual Fall Technical Conference and Exhibition of the Society of Petroleum Engineers of AIME*, Paper No. SPE 11070.

Hartmann T, Wenzel H-G, 1995; The HW95 tidal potential catalogue. *Geophys. Res. Letters,* **22,** 3553-3556; cf R 5.2-11

Jenkins G M, Watts D G, 1968; *Spectral Analysis and its Applications, Holden Day,* San Francisco, 525 pp.; cf R 5.7-12

Larocque M, Mangin A, Razack M, Banton O, 1998; Contribution and correlation of spectral analyses to the regional study of a large karst aquifer (Charente, France). *J. Hydrology,* **205**, 217-231; cf 5.3-13

Le Provost C, Genco M L, Lyard F, Vincent P, Canceil P, 1994; Spectroscopy of the world ocean tides from a finite element hydrodynamical model. *J. Geophys. Res.,* **99,** 24,777-24,798; cf R 5.2-14

Mavko G, Mukerji T, 1995; Seismic pore space compressibility and Gassmann's relation, *Geophysics,* **60**, 1743-1749.

Narasimhan T N, Kanehiro B Y, Witherspoon P A, 1984; Interpretation of the earth tide response of three deep, confined aquifers. *J. Geophys. Res.,* **89,** 1913-1924.

Oppenheim A V, Shafer R W, 1975; *Digital Signal Processing,* Prentice-Hall, Englewood Cliffs, NJ, 505 pp.; cf R 5.7-15

Press W H, Teukolsky S A, Vetterling V T, Flannery B P, 1992; *Numerical Recipes. The Art of Scientific Computing. Cambridge University Press,* 2'nd ed., 963 pp.; cf R 5.7-16

Ray R, 1999; *A Global Ocean Tide Model from TOPEX/POSEIDON Altimetry: GOT99.2,* NASA/TM-1999-209478, National Aeronautics and Space Administration, Goddard Space Flight Center, Greenbelt, MD.; cf R 5.2-17

Robinson M A, Gallagher D L, 1999; A model of ground water discharge from an unconfined coastal aquifer. *Ground Water,* **37**, 80-87; cf R 5.3-18

Rojstaczer S A, Riley F S, 1990; Response of the water level in a well to Earth tides and atmospheric loading under unconfined conditions. *Water Resources Res.,* **26**, 1803-1817; cf R 5.3-11

Rojstaczer S A, Agnew D C, 1989; Influence of formation material properties on the response of water levels in wells to earth tides and atmospheric loading. *J. Geophys. Res.*, **94,** 12,403-12,411; cf R 5.3-19

Scherneck H-G, 1991; A parametrized solid earth tide model and ocean tide loading effects for global geodetic baseline measurements, *Geophys. J. Int.,* **106,** 677-694; cf R 5.2-20

Scherneck H-G, 2001; Solid earth model with liquid core and ocean loading in application to ground water tides in deep wells. In Sato T and Ooe M (eds), *Proceedings 14th International Symposium on Earth Tides, J. Geod. Soc. Japan, special issue,* **47***,* 204-212; cf R 5.2-21

Tiren S A, Askling P, Wanstedt S, 1999; Geologic site characterization for deep nuclear waste disposal in fractured rock based on 3D data visualization. In Talbot C J and Langer, M (eds), *Nuclear waste management and the Earth sciences, Proceedings 9th biannual meeting of the European Union of Geosciences on Nuclear waste management and the Earth sciences, Strasbourg, France, March 25, 1997, Engineering Geology*, **52**, 319-346, 1999.

Unbehauen R, 1971; SystemtheorieEine Einführung für Ingenieure. Oldenburg, München, 224 pp.; cf R 5.7-22

Van der Kamp G, Gale J E, 1983; Theory of earth tide and barometric effects in porous formations with compressible grains. *Water Resour. Res.,* **19,** 538-544; cf R 5.3-23

Wahr J M, 1981; Body tides on an elliptical, rotating, elastic and oceanless earth, *Geophys. J. R. astro. Soc.,* **64,** 677-704; cf R-5.2-11

Wahr J M, Bergen Z, 1986; The effects of mantle anelasticity on nutations, earth tides, and tidal variations in the rotation rate. *Geophys. J. R. astr. Soc.,* **87,** 633-668.

Wahr J M, Sasao T, 1981; A diurnal resonance in the ocean tide and in the earth's load response due to the resonant free 'core nutation'. *Geophys. J. R. astr. Soc.,* **64,** 747-766.

Wanstedt S; Carlsten S; Tiren S, 2000; Borehole radar measurements aid structure geological interpretations, in Allen C T and Plumb R G (eds): *Ground penetrating radar (GPR '98), Proceedings Seventh international conference on Ground penetrating radar, Lawrence, KS, United States, May 27-30, 1998*, *J. Applied Geophysics*, **43**, 227-237.

Wenzel H-G, 1994; Earth tide analysis package ETERNA 3.0. *Bull. d'Inform. Marées Terr.,* **99,** 6813-6855; cf R 5.7-5

Wenzel H-G, 1996; The Nanogal Software: Earth tide data processing package ETERNA 3.30. *Bull. d'Inform. Marées Terr.,* **124,** 9425-9439; cf R 5.6-5

Zaske J, Zürn W, Wilhelm H, 2000; NDFW analysis of borehole water level data from the Hot-Dry-Rock test site Soultz-sous-Forêts. *Bull. d'Inform. Marées Terr.,***132,** 10,241-10,270; cf R 5.3-1

Appendix

5 Appendix A: Review of literature

5.1 Elasticity, Poro-elasticity

Wang H, 1993; Quasi-static poroelastic parameters in rock and their geophysical applications. *Pure Appl. Geophys.*, **141**, 269-286.

not seen

Kümpel H-J, 1991; Poroelasticity: parameters reviewed. *Geophys. J. Int.,* **105,** 783-799.

Starts with the general formulations from the theory of Biot, the stress-strain relations, Darcy's flow law, constitutive equations of poroelasticity, mechanical rock properties and relations between drained and undrained elastic parameters. Next section is on the phenomenological approach, reviewing parameters' relations to pressure and volume changes and discussing parameters that characterise storage properties. Follows a section on diffusive relations for pressures. The definition and meaning of the significant parameters of poroelasticity are given in a central table. Special cases of anisotropy, nonlinearity, inelasticity, rapid pressure changes and thermal effects are covered in short paragraphs with many references to literature where more focussed studies are reported. The reference list contains altogether 115 items.

Rice J R, Cleary M P, 1976. Some basic stress diffusion solutions for fluid-saturated elastic porous media with compressible constitutents. *Rev. Geophys. Space Phys.,* **14,** 227-241.

Fundamental work on the problem of pressure diffusion and diffusion-controlled flow of fluids in porous media.

R 5.1-1

Nur A, Byerlee J D, 1971; An exact effective stress law for elastic deformation of rock with fluids. *J. Geophys. Res.,* **26,** 6414-6419.

Fundamental work on the deformation of fluid-filled porous media.

5.2 Tides

A general bibliographic database on tides is available at
http://www.astro.oma.be/ICET/icetdb/icetdb.html

5.2.1 Astronomical tides

The following literature is standard to astronomical tides and their numerical treatment:

R 5.2-1

Melchior P, 1987; *The Tides of the Planet Earth,* Pergamon, Oxford, 609pp.

Standard text book in the field of tides and astronomical nutation, the phenomena, the analysis, and instruments. And a large bibliography.

Cartwright D E, 1998; *Tides – a Scientific History,* Cambridge University Press, Cambridge, UK., 304 pp.

A historical summary covering the discovery of the phenomena, their understanding and the emergence of their mathematical-physical formulation. A certain degree of emphasis on oceanic tides.

Wilhelm H, Zürn W, Wenzel H-G, 1997; *Tidal Phenomena,* Lecture Notes in Earth Science, Vol. 66, Springer, Berlin, 398 pp.

Contains chapters on: Earth Tides. - Ocean Tides and Related Phenomena.– Atmospheric Tides and Related Phenomena. - Tidally Induced Phenomena. - Tides on Planets and Stars. Problems of geodynamics in the discussion of the late 80'ies to early 90'ies are discussed in a general setting. The lecture notes provide the physical mathematics needed to describe and understand the phenomena. The text includes open questions and eventually dead-end roads (causes of the observed anomalous pole tide for instance) and is therefore more like lecture notes from a seminar or summer school than a timeless textbook. Concentrating on the background material, the book can provide the fill-in for gaps of understanding for a casual follower of the subject area. A chapter on tides in water-saturated media by Kümpel is referred to in section 3.2.4 below.

R 5.2-2

Cartwright D E, Tayler R J, 1971; New computations of the tide-generating potential. *Geophys. J. R. Astron. Soc.,* **23,** 45-74.

Cartwright D E, Edden A C, 1973; Corrected tables of tidal harmonics. *Geophys. J. R. Astron. Soc.,* **33,** 253-264.

For a long time this was the basic reference tide potential development. The catalogue comprises almost 500 different tide frequencies and develops the spherical harmonics up to degree and order 3.

R 5.2-3

Tamura Y, 1987; A harmonic development of the tide-generating potential. *Bull. d'Inform. Marées Terr.,* **99,** 6813-6855.

This harmonic development contains almost 1200 different tidal waves, including the leading effects from Venus and Jupiter. It develops the spherical harmonics up to degree and order 4.

R 5.2-4

Hartmann T, Wenzel H-G, 1995; The HW95 tidal potential catalogue. *Geophys. Res. Letters,* **22,** 3553-3556.

A recent harmonic development of the tide potential with 12935 partial tides.

5.2.2 Surface loading problem

R 5.2-5

Farrell W E, 1972; Deformation of the earth by surface loads, *Rev. Geophys. Space Phys.,* **10,** 761-797.

This is the leading reference to the loading problem. The concept of load Love numbers for an elastic spherical planet is used, from which the point-load Green's functions are computed. The loading effect at a point due to a global mass distribution is computed by a finite approximation to the convolution integral.

R 5.2-6

Scherneck H-G, 1991; A parametrized solid earth tide model and ocean tide loading effects for global geodetic baseline measurements, *Geophys. J. Int.,* **106,** 677-694.

Scherneck H-G, 2001; Solid earth model with liquid core and ocean loading in application to ground water tides in deep wells. In Sato T and Ooe M (eds), *Proceedings 14th International Symposium on Earth Tides, J. Geod. Soc. Japan, special issue,* **47***,* 204-212.

The tide loading computations in this work use gridded loading fields with refinement in the near-zone of the load. The 1991 article covers only vertical and horizontal displacement. For strain see the 2000 article.

R 5.2-7

Matsumoto K, Sato T, Takanezawa T, Ooe M, 2000; GOTIC2: A program for computation of oceanic tidal loading effect. In Sato T and Ooe M (eds), *Proceedings 14th International Symposium on Earth Tides, J. Geod. Soc. Japan, special issue,* **47**, No. 1, 243-248.

The NAO tidal prediction system GOTIC2 can be downloaded from the National Astronomical Observatory of Japan internet server under
http://www.miz.nao.ac.jp/staffs/nao99/index_En.html

R 5.2-8

Agnew D C, 1997; NLOADF: A program for computing ocean-tide loading. *J. Geophys. Res.,* **102,** 5109-5110.

The program can be obtained by contact with Duncan C. Agnew at Scripps Institute of Oceanography, San Diego, CA.

5.2.3 Ocean tides

Ocean tide models are needed to compute ocean loading effects in the strain components. These effects can be large near coasts of tidal basins, but even far away the effect can be noticeable.

Ocean tide models can be obtained on the following medium:

CD-ROM “A Collection of Global Ocean Tide Models” from JPL, http://poodac.jpl.nasa.gov, Jet Propulsion Laboratory, Physical Oceanography Distributed Active Archive Center.

Two publications are mentioned because of their impact:

R 5.2-9

Le Provost C, Genco M L, Lyard F, Vincent P, Canceil P, 1994; Spectroscopy of the world ocean tides from a finite element hydrodynamical model. *J. Geophys. Res.,* **99,** 24,777-24,798.

a high-resolution hydrodynamic model with emphasis on shelves and little yield to observations (no formal data inversion or assimilation), and

R 5.2-10

Ray R, 1999; *A Global Ocean Tide Model from TOPEX/POSEIDON Altimetry: GOT99.2,* NASA/TM-1999-209478, National Aeronautics and Space Administration, Goddard Space Flight Center, Greenbelt, MD.

as a recent high-quality model assimilating satellite altimetry.

Andersen O B, Woodworth P I, Flather R A, 1995; Intercomparison of recent ocean tide models. J. Geophys. Res., 100, 25,261-25,282.

This is a comparison of results after the first two years of TOPEX/POSEIDON Satellite Altimetry of the oceans.

5.2.4 Strain tides

R 5.2-11

Wahr J M, 1981; Body tides on an elliptical, rotating, elastic and oceanless earth, *Geophys. J. R. astro. Soc.,* **64,** 677-704.

The Wahr (1981) thesis on the planetary response to tidal forces is applicable to most observable tide effects, including strain. It is developed for an earth model that is rotating, elliptic with a liquid core and an elastic mantle and crust according to the 1066A earth model of Gilbert and Dziewonski (1975). It is an oceanless model. Later extensions to anelasticity in the mantle focussed on gravity and displacement components (Wahr and Bergen, 1986). Excitation of the nearly-diurnal free motion of the core due to tidal forces from both luni-solar and oceanic origin were considered by Wahr and Sasao (1981). One assumption in Wahr's model is that inner surfaces in the earth would coincide with equipotential surfaces. As we know today, the core-mantle boundary is displaced from this equilibrium position, which has a noticeable effect on the exact frequency of the liquid core's free wobble (one beat period in 460 days in Wahr's (1981) model versus a 435 days beat period that is observed).

Westerhaus M, Zürn W, 2001; On the Use of Earth Tides in Geodynamic Reseach, *J. Geodetic Soc. Japan, spec. issue,* **47**, No. 1

This work includes general properties of media responding to strain, like porous media, well efficiency variations, also in geodynamically active regions. A reprint may be obtained from the authors (Westerhaus at GfZ, Potsdam, Zürn at University Karlsruhe/BFO Schiltach).

Ozawa I, 1998; Observations of the earth tide vertical extension in the old Osakayama Tunnel. *Bull. d'Inform. Marées Terr.,* **130**, 10,064-10,075

Article is important in the aspect of vertical extension in the crust near the surface, which in the luni-solar tidal problem is regarded as stress-free. Only few such *in situ* studies are available. Ozawa obtains for the expression $d(ah_2)/dr = -1.38$ (0.036% reduction at 1 km depth with respect to surface value). However, important contributions to vertical strain from solar heating of the surface and barometric loading at solar-synchronous cycles are observed.

Theory concerning tidal stress in the interior of the earth is also presented

Varga P, Grafarend E, 1996; Distribution of the lunisolar tidal elastic stress tensor components within the Earth's mantle. *Phys. Earth Planet. Int.,* **93**, 285-297.

Hart R H G, Gladwin M T, Gwither R L, Agnew D C, Wyatt F K, 1996; Tidal calibration of borehole strain meters: Removing the effect of small-scale inhomogeneity. *J. Geophys. Res.,* **101,** 25,553-25,771.

This is in part a reverse problem formulation. The diameters of a borehole are precisely and carefully measured as an indicator of strain ("tensor strain meters"). Only the components in the plane perpendicular to the borehole are observable. The study uses 3x3 coupling matrices between observed strain meter channels and regional elements of the strain tensor. While tectonic strain in California is an important parameter in conjunction with earthquake research. Tidal strain is relatively well-known on the regional scale. Ocean loading strain due to the tides mostly in the Pacific is modelled using global tidal charts. The combined, modelled tide strain is used to calibrate the strain meters. The test site is the Piñon Flat geophysical observatory, southern California. Effects of larger seismic events (Landers and Big Bear in 1992) are observed. Strain is also observed in collocated laser strain meters and is compared with the borehole measurements. Solutions and observations are characterised by the authors as well consistent.

5.3 Well tides

5.3.1 Tides in fractures in crystalline rock

Literature that show observation of tides in fractures in crystalline rock is relatively numerous, however less in number than in the case of porous media. Literature in this range of applications may be limited mainly because the water-bearing structures are not delivering large volumes of fluid, while deep boreholes are expensive; therefore, this kind of research is difficult to fund. There are ground-breaking studies by Bower and by Hanson, which have been applied to special borehole studies often in conjunction with scientific studies of rock materials at great depth, e.g. the Continental Deep-Drilling project in Germany.

Kümpel H-J, 1997; Tides in water-saturated rock, in Wilhelm H, Zürn W, Wenzel H-G (eds): *Tidal Phenomena,* Lecture Notes in Earth Science, Vol. 66, Springer, Berlin.

Treats tidal and barometric efficiency of wells, considering mostly isotropic (small-scale) poroelasticity in the analysis. Points out that saturation with pore fluid is needed to produce observable signal in tidal water pressure change. Also discusses the difficulty to estimate a porosity parameter. The possibility to estimate the following parameters is discussed: Skempton's parameter and the undrained Poisson ratio, assuming one of the following parameters is known: the compressibility of the rock material forming the matrix or the ratio of horizontal to vertical strain. Distinguishes the porous case from flow through large fractures, the latter theme being covered with several references.

R 5.3-1

Zaske J, Zürn W, Wilhelm H, 2000; NDFW analysis of borehole water level data from the Hot-Dry-Rock test site Soultz-sous-Forêts. *Bull. d'Inform. Marées Terr.,* **132,** 10,241-10,270.

This article studies 2 years of data from the 2002 m deep well in the Rhinegraben area in NW France. The well is not packed, water head at 39 m depth, sensed at 45 m depth with a piezometer. The tides can be resolved in amplitude at 0.1% of the full range. The piezometer signal has been sampled at 10 min intervals. For pressure loading studies records from a barometer at the site and another one at Karlsruhe 30 km to the east are used. Generally, the tidal variations in this well are small-scaled (1 cm). At several times, the measurement conditions were disturbed due to ongoing hydraulic testing. Nevertheless the authors succeed to resolve the resonance of the liquid earth core in the diurnal tide spectrum. Some small tidal waves important for this analysis are determined at a 5σ level of significance. The authors point out ocean tide loading as an important effect that must be accounted for if parameters for the resonance are to be estimated.

Limitations in the tidal study that Zaske et al. (2000) point out can conversely be treated as demonstration of sensitivity to formation parameters. The response does change character over time, which may be taken as evidence for changes in confinement conditions. The diurnal solar cycle appears to interfere with the P_1 tide.

This study does not attempt to solve for parameters characteristic of the hydrogeology of the well, but the authors document their awareness of existing methods.

First tide studies of this site date back to a Diploma thesis by S Mohr and S Frey, unpublished manuscript at Institute of Geophysics, University of Karlsruhe, 1991 (unseen).

R 5.3-2

Endom J, Kümpel H-J, 1994; Analysis of natural well level fluctuations in the KTB-Vorbohrung - Poroelastic aquifer parameters and single fracture models. *Scientific Drilling*, **4**, 147-162.

This article analyses temporal variations of water level in the polite hole of the continental deep drilling project (KTB-VB = *Kontinentale TiefBohrung - Vorbohrung*) between January and December 1992 in the Bohemian massive near Windisch-Eschenbach, Bavaria, Germany. The hole is 4000.1 m deep and cased except for the depth interval between 3850 and 4000 m. The authors consider the fracture models of Bower (1983) and Hansen and Owen (1982) as well as porosity models and extends to flow properties in these structures in order to explain the observed gain factors and phase lags. The sensing method is similar to Zaske et al. (2000) above, namely water depth is sensed with an immersed piezometer some tens of metres below the water surface. As excitation sources again, tides and air pressure loading of the crust are considered. The tide phase shifts are analysed with the fracture zone parameters. The analysis of the observations determines the following parameters: the effective width across the fracture and the lateral diameter of the fracture zone (height and length in the bi-wing model of Hansen, 1983); dip and azimuth angle. The following hydrogeological parameters were estimated: in the porous assumption, the Skempton parameter, specific storage coefficient, and porosity; in the single-fracture assumption, permeability and transmissability. For the hydrogeological quantities, rock parameters from laboratory measurements were used (compressibility, Poisson ratio).

The following papers are central to this investigation. While the Bower group supposes a penny-shaped fracture zone with orientation parameters for dip and azimuth, the Hanson monograph considers application to a vertical, bi-wing-shaped fracture zone:

R 5.3-3

Bower D R, 1983; Bedrock fracture parameters from the interpretation of well tides, *J. Geophys. Res.,* **88,** 5025-5035

R 5.3-4

Bower D R, Van der Kamp G, Gale J E, 1983; Fracture parameters revealed by earth tides and barometric effects in crystalline rock, in Kuo J T (ed.) *Proceedings 9'th International Symposium on Earth Tides,* pp. 631-639, Schweizerbart'sche Verlagsbuchhandlung, Stuttgart.

R 5.3-5

Hanson J M, 1983; *Evaluation of subsurface fracture geometry using fluid pressure response to solid earth tidal strain.* TerraTek TR83-26, Terra Tek Inc., Salt Lake City, Ua. 135pp.

Hanson J M, Owen L B, 1982; Fracture orientation analysis by the solid earth tidal strain method. In: *Proc. 57'th Annual Fall Technical Conference and Exhibition of the Society of Petroleum Engineers of AIME*, Paper No. SPE 11070.

The case of oriented fractures studied here implies that skin depth of the flow can be neglected and transmissivity is high. In this case the stress normal to the crack wall is transmitted to the water. The finite radius of the void (length times height) creates a small pressure term that is proportional to the shear modulus of the rock formation. It reflects the widening of the fracture under compression along the axes in the fracture plane. Both of these studies concentrate on the lunar tides O_1 and M_2 as being strong tidal effects and not noticeably affected by environmental perturbations. The information contained in these tides is sufficient to simultaneously resolve four parameters. Drawdown effects of the well should be avoided in order to preserve the amplitude ratio of the tidal waves in the ambient strain field. The theory is employed in Chapters 1 and 2 of this report.

Duguid J O and Lee P C Y, 1977; Flow in fractured porous media. *Water Resour. Res.,* **13**, 558-566.

Not seen. Referred to by Kümpel (1997) as pioneering work on the deformation of fluid-filled cracks.

R 5.3-6

Marine I W, 1975; Water level fluctuations due to earth tides in a well pumping from slightly fractured rock. *Water Resour. Res.,* **11,** 165-173.

In a study for the Atomic Energy Commission the Savannah River environment was studied in aspects of the different ground water systems found in the area. One well of this study is driven into the crystalline basement (metamorphic rocks, schists and gneisses). The concept of Bredehoeft (1967) is used to estimate porosity from tides and barometric efficiency. The specific storage parameters are taken from pumping tests. Comparison of theoretical tide effect (gravity potential) and observations show almost no phase shifts. Data set do not suggest that oriented fractures are important in this well. The other ground water systems seem to be unconfined, showing almost no tidal response.

5.3.2 General aquifer studies

Smith T E, 1994; Analysis of tidal fluctuation effects on a confined and unconfined aquifer. *Proc. 1994 Focus conference on Eastern ground water issues,* National Ground Water Association, USA, pp.757-771.

not seen

Ritzi R W, 1989; *The Use of Well Response to Natural Forces in the Estimation of Hydraulic Parameters,* PhD Thesis, Dep. Hydrology and Water Resources, University of Arizona. UMI Dissertation Services, Ann Arbor, Michigan, 235 pp.

This thesis emphasises the problem of parameter estimation from the frequency response functions obtained from spectrum analysis of water head records, earth tides and barometric pressure. The aquifer type treated is a confined horizontal, porous layer of constant thickness. The two excitation sources are treated both separately and in a joint model. The thesis considers estimation algorithms (Gauss-Markov, Monte Carlo) and is careful on uniqueness and identifiability of parameters. The basic form of well response considered is the one modified by well drawdown, i.e. long-period response is low since flow is limited, and high-frequency response approaches a real-valued parameter determined by transmissivity T and storativity S. The frequency response curve becomes a function of the dimensionless number T/fr^2 with S as a parameter. From the frequency response curves (distinguished into amplitude and phase) the parameters T and S are estimated.

Roeloffs E A, 1988; Hydrologic precursors to earthquakes - a review. *PAGEOPH,* **126,** 177-209.

Contains a compilation of M_2 tide observations in a large number of wells (not seen)

Hsieh P A, Bredehoeft J D, Farr J M, 1987; Determination of aquifer transmissivity from earth tide analysis, *Water Resour. Res.,* **23,** 1824-1832.

Authors estimate transmissivity and storativity of wells using tidal observations. The limited flow to the well bore causes phase shift between strain tide in the aquifer and water head variation. Tries to avoid barometric problem throughout. The storage coefficient is found to influence the response only slightly. The key parameter that can be observed is transmissivity. The well analysed is near Parkfield, California

Sterling A, Smets E, 1971; Study of earth tides, earthquakes and terrestrial spectroscopy by analysis of the level fluctuations in a borehole at Heibaart (Belgium). *Geophys. J. Roy. Astr. Soc.,* **23,** 225-242.

Early study on tides in water wells with focus on the borehole measurement for geodynamic research (very wide-band seismic spectroscopy). Borehole is cased down to 1480 m depth. This length transsects 1029 m of top soil and cenozoic to cretaceous sediments and 451 m of a crystalline, cracked zone, which is tapped between 1480 and 1638 m depth. Earth tide harmonic analysis is carried out estimating parameters that relate water level oscillations to gravity. Amplification effect of well tide to the fluid core free wobble is studied at detail. Loading effect of near-by British Channel is mentioned as a perturbation. More work on this is announced but I was unable to locate the publication. Sterling and Smets show examples of distant earthquakes (e.g., Peru, May 31, 1970) that were recorded in the water level in this well.

R 5.3-7

Bredehoeft J D, 1967; Response of well-aquifer systems to earth tides. *J. Geophys. Res.,* **72,** 3075-3087.

Early paper on the subject. Considers the draw-down effect near the well and the drainage flow as the main amplitude-effective property. Develops the formulas for this effect which reappear in later work with relatively little modification. Confined and unconfined cases are shown and the latter explained as tidally inefficient. Tide analysis of five different tide waves in three different wells (Belgium, Iowa, New Mexico). Barometric efficiency is estimated. Does consider elastic deformation of the soil skeleton. Bredehoeft also presents a summary of papers from 1880 to 1967 with observations of tides in wells and attempts to study solid earth deformation and rock parameters.

5.3.3 Confined aquifers

This is the most intensively covered section. It concerns the simplified case of approximately horizontal-isotropic, homogeneous aquifers in confined or nearly-confined conditions. Tides in fractures above can be seen as a special case of singular, geometrically oriented systems of voids with significant inhomogeneity. Confined aquifers will at some scale comprise a large ensemble of such fracture systems where orientation effects are less important.

Wakahama H, Akita F, Matsunami T, 1997; On hydraulic coefficients estimated from water level fluctuations of deep confined geothermal wells; case study of Shintotsukawa geothermal wells. *Reports of the Geological Survey of Hokkaido,* **68**, 81-97.

Tides are analysed in this report using methods of Bredehoeft (1967). Compares mean specific storage coefficient from interference test with tide analysis results and finds reasonable agreement. Evidence exists that tide response is different in the different frequency bands, and anisotropic conditions in the aquifer must be assumed.

Bredehoeft, J D, 1997; Fault permeability near Yucca Mountain. *Water Resources Res.,* **33**, 2459-2463.

Investigates conditions near the proposed US American nuclear waste deposite site. Confinement conditions are assessed by means of the earth tide response. Comparisons of well heads at different depth indicate the effect of a sharp rise in temperature across boundaries between aquifers. Of major concern is a carbonate layer that contains the aquifer with the higher temperature. Permeability and hydraulic conductivity of an intervening fault are modelled and the resulting tidal head variations compared to observations in an 1100 m deep borehole. The aquifer seems to be quite tight, but the fault zone may have an important level of conductivity. Changing the well heads by underground work could imply important changes of confinement conditions for the carbonate aquifer which subsequently will become enriched in radionuclide content.

Pinilla J F, Trevisan O V, Tinoco F L, 1997; Coupling reservoir and geomechanics to interpret tidal effects in well tests. *1997 SPE annual technical conference and exhibition; Formation evaluation and reservoir geology, Part II, Society of Petroleum Engineers of AIME, 1997,* pp. 301-314.

Interesting title - not seen, no abstract available.

Marsaud B, Mangin A, Bel F, 1993; Estimation des caractéristiques physiques d'aquifères profonds à partir de l'incidence barométrique et des marées terrestres. *J. Hydrology,* **144**, 85-100 (in French).

Six different tide waves are considered (including the fortnightly M_f). Porosity and storage coefficients are estimated. Authors use cross-spectral time series analysis methods. Correlation with air pressure yields gain, phase, and coherency spectra. Equivalent for tide component. Application to data from Betbezer borehole in cretaceous limestone, south-west France.

Ozawa I, 1992; Observations of the earth tidal strains in the directions NS at Suhara on the coast. *J. Geodetic Soc. Japan,* **38**, 251-257.

Report shows residual influence of ground water variations on strain measured by borehole cross-section deformation. The ground water tides are assumed to be dominated by oceanic tide loading along the coast.

Rojstaczer S, 1993; Ground water level changes associated with seismicity in the Anza region, San Jacinto Fault, California.

GeoRef record appears incomplete; abstract available. Abstract describes that tides and barometric pressure relations are used to calibrate the strain response. Five wells are studied and twelve moderately sized earthquakes. Notes strongly frequency-dependent barometric response.

Igarashi G, Wakita H, 1991; Tidal responses and earthquake-related changes in water level of deep wells. *J. Geophys. Res.,* **96**, 4269-4278.

Eight tidal frequencies considered. Two wells under study (100 m, 500 m depth) are near the coast of Japan, and ocean tide loading is considered as an important source of aquifer strain, roughly 1/2 in magnitude of the solid earth tide strain. The deeper well shows much larger tide strain efficiency (4 times), both show roughly the same barometric efficiency. Coseismic events in the form of water level steps are observed in two out of five cases, ranging at the centimetre level. Removal of tide and barometric effect is vital to discriminate tectonic signals.

Liu Guoshou, 1998; Water level short-impending anomaly in Yunnan No. 05 well before earthquakes. *J. Seismol. Res.,* **21**, 282-285. (English title and abstract, article in Chinese)

Zhang Zhaodong, Zheng Jinhan, 1993; Response of water level in deep well to Earth tide and barometric pressure. *J. Seism. Res.,* **16**, 431-438.

Citations are representative for a large number of papers in the Chinese literature studying to use ground water observations to monitor stress and strain, partly in application to earthquake prediction. The solid earth tides are removed from the signals in these studies with the astronomical response or with frequency filter methods. Sometimes, tide anomalies are observed and correlated with seismotectonic events. Related journals running articles on the subject: *Seismology and geology; Earthquakes; Acta Geophysica Sinica.*

R 5.3-8

Evans K, Beavan J, Simpson D, 1991; Estimating aquifer parameters from analysis of forced fluctuations in well level: An example from the Nubian formation near Aswan, Egypt. 1. Hydrogeological background and large-scale permeability estimates. *J. Geophys. Res.,* **96,** 12,127-12,137.

Beavan J, Evans K, Mousa S, Simpson D, 1991; Estimating aquifer parameters from analysis of forced fluctuations in well level: An example from the Nubian formation near Aswan, Egypt. 2. Poroelastic properties. *J. Geophys. Res.,* **96,** 12,139-12,160.

Evans K, Beavan J, Simpson D, Mousa S, 1991; Estimating aquifer parameters from analysis of forced fluctuations in well level: An example from the Nubian formation near Aswan, Egypt. 3. Diffusivity estimates for saturated and unsaturated zones. *J. Geophys. Res.,* **96,** 12,161-12,191.

This three-paper series explores the Nubian sandstone formation near Aswan and lake Nasser. The sandstone is characterised by high porosity (up to 0.3). The hydrogeology is studied in five boreholes typically 100 m deep. Both the tidal and atmospheric pressure responses are employed.

Ritzi R W, Sorooshian S, Hsieh P, 1991; The estimation of fluid flow properties from the response of water levels to the combined atmospheric and earth tide forces. *Water Resour. Res.,* **27**, 883-893.

Application to aquifers in sedimentary rocks, shallow depth, confining overburden. Computes formation pressure and dilatation from a combination of air pressure and tides in order to obtain a wider excitation spectrum than from air pressure alone. Frequency response curves are shown to have important transition properties between different regimes across this frequency band.

R 5.3-9

Rojstaczer, S, Agnew D C, 1989; Influence of formation material properties on the response of water levels in wells to earth tides and atmospheric loading. *J. Geophys. Res.*, **94,** 12,403-12,411.

This is an important study. The authors consider porous media in the limit where flow exchange with the well can be neglected and the porous formation is confined. This situation, termed the **static-confined** case, is an idealised end member of more realistic situations where flow within the aquifer is important to some degree. In particular, since horizontal strain in homogeneous porosity is homogeneous and therefore incapable to drive horizontal flow, only vertical flow will occur as a consequence of vertical changes in the formation, or as a consequence of (zero-) pressure boundary conditions, for instance if the deep aquifer is weakly connected to drained sections like the phreatic surface. In this situation the authors speak of pressure diffusion. They show that different responses apply in the tidal case and in the pressure loading case. Observing the responses (tidal efficiency, barometric efficiency) can reveal governing parameters, mainly drained compressibilty and porosity). Application is to Mammoth Lake and Parkfield wells in California.

R 5.3-10

Van der Kamp G, Gale J E, 1983; Theory of earth tide and barometric effects in porous formations with compressible grains. *Water Resour. Res.,* **19,** 538-544.

Important theory and review paper. Shows the problems of tide- or surface-load driven groundwater pressure variations in crystalline rocks of low porosity, where Bredehoeft (1967) usually overestimates transmissivity and porosity. Considers mainly subhorizontal, homogeneous aquifers with negligible horizontal flow. The vertical flow induced by stress in the aquifer is treated as a one-dimensional diffusion problem. The paper concentrates on the role of the elastic solid and its parameters as being the confining body.

Bodvarsson G, 1970; Confined fluids as strain meters, J. Geophys. Res., 73, 2711-2718.

Considers high-frequency excitation as e.g. from seismic events and therefore studies the impact of the inertia of the fluid. Studies flow in a porous medium. Computes skin depths for tides and for Rayleigh waves, i.e. how wide a radius around the well is contributing to the water head variation in the well.

5.3.4 Unconfined or partially confined aquifers

The majority of publications concerning tides in wells study unconfined aquifers. Some of these have bearing on confined cases. The following list is to represent only this narrower range.

R 5.3-11

Rojstaczer S A, Riley F S, 1990; Response of the water level in a well to Earth tides and atmospheric loading under unconfined conditions. *Water Resources Res.,* **26**, 1803-1817.

Considers a thick aquifer that responds to tide strain and by vertical flow exchanges water with an unsaturated, shallow zone. The frequency spectrum of barometric efficiency is shown to go through a range of curve types depending on a parameter signifying the variations in the water table

Rojstaczer S A, 1988; *The Response of the Water Level in a Well to Atmospheric Loading and Earth Tides: Theory and Application.* PhD Thesis, Dep. Applied Earth Sciences, Stanford Univ., Stanford, California. UMI Dissertation Service, Ann Arbor, Michigan, 211 pp.

Covers the physics of deformation and flow in porous rocks. Notes the static-confined response as an end-member of typical conditions where both drawdown (drainage) effects and unconfined conditions modify the response, the former in the long-period and the latter in the high-frequency domain. Most significant contribution is the

consideration of a water table above the deep aquifer. Also in this study, aquifers considered are horizontal layers with more or less permeable overburden and bottom. Three wells are surveyed, all located near the San Andreas fault in California. Thesis notes the possibility of an enhanced barometric efficiency by air diffusion effects. Many ideas laid down in this thesis have gone into the article by Rojstaczer and Agnew (1989).

R 5.3-12

Baird A J, Mason T, Horn D P, 1998; Validation of a Boussinesq model of beach ground water behaviour. *Marine Geology,* **148,** 55-69.

Robinson M A, Gallagher D L, 1999; A model of ground water discharge from an unconfined coastal aquifer. *Ground Water,* **37**, 80-87.

Ross B, 1999; Tidal inflow to aquifers. *Water Resources Res.*, **35**, 3967-3968.

Trefry M G, Johnston C D, 1998; Pumping test analysis for a tidally forced aquifer. *Ground Water*, **36**, 427-433.

Intersection of aquifers with oceanic tidal regimes, e.g. estuaries. There are more articles in the literature, but since subject is only of marginal interest, the list is discontinued.

The problem of tidal inflow can be of principal interest in the case of shallow fractures that continue into a tidal basin. In the Baltic Sea with its low tide range this problem is probably negligible.

R 5.3-13

Hsieh PA, Bredehoeft J D, Rojstaczer S, 1988; Response of well aquifer systems to earth tides: Problem revisited. *Water Resour. Res.,* **24,** 468-742.

This is a rebuttal to an objection by Narasimhan et al (1984) concerning the extrapolation of specific storage estimates to drained conditions, which would be the reference state for specific storage. Earth tides would not involve drainage to any noteworthy degree and thus are unsuitable for drainage-related parameters. Therefore the analyses based on this approach, including a large number of studies after Bredehoeft (1967) would be internally inconsistent. The rebuttal reinforces the method originally proposed by Bredehoeft (1967) and demonstrates its consistency. The discussion in Hsieh et al reviews important concepts applying to tides in elastic rock matrices.

Westerhaus, M., 1996: *Tilt and well level tides along an active fault. A contribution to the joint German-Turkish project on earthquake research.* GeoForschungsZentrum Potsdam, Scientific Technical Report, STR96/05, 265 p.

Not seen.

5.3.5 Hydrothermal wells

Calo G C, Tinelli R, 1995; Systematic hydrological study of a hypothermal spring (S. Cesarea Terme, Apulia), Italy. *J. Hydrology,* **165**, 185-205.

Shows presence of a.o. tidal fluctuations and effects on chemistry.

R 5.3-14

Larocque M, Mangin A, Razack M, Banton O, 1998; Contribution and correlation of spectral analyses to the regional study of a large karst aquifer (Charente, France). *J. Hydrology,* **205**, 217-231.

Example is from a Karst aquifer, apparently unconfined but due to the finding of tides argued to show confined behaviour. Observed parameters are flow rates, piezometric levels, electrical conductivity, water temperature, air pressure and precipitation.

5.4 Barometric

R 5.4-1

De Vries J J, Gieske A 1988; Barometric tides in partly-saturated confined aquifers in Botswana. *J. Hydrology,* **104**, 17-32.

Water level variations at periods of 24h and integer fractions down to 6h are observed in fracture aquifers that are partially saturated. The aquifers of the study are overlain by more impervious layers that thus isolate them from direct atmospheric influence. The water level variations are shown to result from interaction between the pressure on the well head and the ambient pressure around the aquifer, implying water exchange with the well by flow. The paper employs harmonic analysis to demonstrate systematic relations of amplitudes and phase shifts between the air pressure and well level records. The aquifer is characterised by high porosity and low conductivity, which appear to explain the relatively large barometric effects.

Desbarats A J, Boyle D R, Stapinsky M, Robin M J L, 1999; A dual-porosity model for water level response to atmospheric loading in wells tapping fractured rock aquifers. *Water Resour. Res.,* **35**, 1495-1505.

(review pending)

5.5 Seismotectonic

This section reviews material with main application to seismology and fault movement. Many of the articles employ tide analysis in order to constrain time- or frequency-dependent response models for the well and its coupling to the ambient strain field.

Masterlark T L, Wang H F, Chan Lung S, Che Yongtai, 1999; Coseismic fluid-pressure response estimated from prediction-error filtering of tidal band loading. *Bull. Seism. Soc. Am.,* **89**, 1439-1446.

Method aims at removal of barometric and tidal signals from ground water pressure records to retain and enhance pressure changes related to tectonic, in particular coseismic influences. The method does not require explicit computation of astronomical tides. Barometric effects are generally described as a convolution product; in the article only one constant admittance coefficient is used, however. Two wells are used, located in north-east China. One of them is in carbonate rock, 3402 m deep, the other in andesite tuff, 362 m deep. Three years of data have been analysed.

R 5.5-1

Ágústsson K, Linde A T, Stefánsson R, 1999; Strain changes for the 1987 Vatnafjöll earthquake in south Iceland and possible magmatic triggering. *J. Geophys. Res.,* **104,** 1151-1161.

Ágústsson et al. have also observed tides in their network of Sacks-Evertson borehole volume-strainmeters in the Southern Iceland Seismic Zone. Ocean loading tides in the strain component are large at these sites. The work is interesting in the current context since the strainmeters can be installed in boreholes in dry sections. The high dynamic range of the sensor and experience from signal processing are shown.

Kitagawa G, Matsumoto N, 1996. Detection of coseismic changes of underground water level. *J. Am. Stat. Assoc.*, **91**, 521-528.

Removal of tide signals from water level records using astronomical tide computations and response method.

Kissin I G, Belikov V M, Ishankuliev G A 1996; Short-term groundwater level variations in a seismic region as an indicator of the geodynamic regime. *Tectonophysics,* **265**, 313-326.

A descriptive paper (no theory) investigates transient water level changes in an array of 23 boreholes near the Main Kopetdag fault, Turkmenistan, and relations with seismic events in the zone. The rocks in the area are limestone, dolomites and sandstone. For each earthquake, deformation is estimated (strain magnitude). For each well event, a candidate earthquake in the vicinity is associated occurring within a certain time window (apparently ±12 h). Several well events have no earthquake report. More events occurring pre-seismically than co-seismically are reported. The group of largest well events are all found to be preceding the seismic events. Tide amplitudes are used to characterise the hydraulic coupling of the well to the deformation field. Systematic decrease of tide amplitudes with increasing distance from the Main Kopetdag Fault appears indicated.

Leonardi V, Arthaud F, Tovmassian A, Karakhanian A S 1997; Relationships between seismic activity and piezometric level changes in the Arax basin (SW Armenia); attempt at a typology of seismically induced piezometric anomalies. *Tectonophysics,* **273**, 293-316.

Investigation of the relation between seismic deformation and effects on pressure in an aquifer. Rocks are gravels (partly with crystalline blocks), sands, and clays. Area is sampled with 100+ piezometers. Two wells are observed for water table changes. Maps of seismic activity (event density); filtering of the piezometric record to enhance discrimination of events. Barometric corrections use the method of Van der Kamp and Gale (1983). One well was tested is to whether tidal corrections are required; the outcome is clearly negative.

R 5.5-2

Roeloffs E A, Schulz Burford S, Riley F S , Records A W, 1989; Hydrologic effects on water level changes associated with episodic fault creep near Parkfield, California. *J. Geophys. Res.,* **94,** 12,384-12,402.

The water level in a 460 m deep well is observed for episodic changes in relation to events on the San Andreas fault near Parkfield, California. Two fluid reservoirs exist at 85 and 250 m depth and are measured independently. Flow to the well bore is important in this well. The article notes strain changes in the long-term are coupled in a different relation to observed well level changes compared to the transients on scales of less than one to several days that are in the focus of the paper. Since tides play an intermediate role in this period range, dynamic relations between regional strain and water level changes are based in tide-derived parameters.

5.6 Ground water as a source of perturbation of geodynamic instruments (gravimeters, tilt meters)

Mentes G, Varga P, Kümpel, H-J, 1999. Recording of recent crustal movements by borehole tiltmeters in the vicinity of a tectonic fault. *Bull. d'Inform. Marées Terr.,* **131**, 10,207-10,215.

The level of perturbation is controlled predominantly by the mass of water encompassed in the motion. Most of these studies are carried out in sedimentary areas where the fraction of pore volume is large. Volume 131 of *Bull. d'Inform. Marées Terr.* is a special issue devoted to environmental influences on earth tide instruments.

Mäkinen J and Tattari S, 1991; The influence of subsurface water storage on observed gravity, In: Proc. Eleventh Int. Symp. Earth Tides, J Kakkuri (ed), pp. 457-471.

and…

R 5.6-1

Delcourt-Honorez M, 1986; Earth tide response and barometric effect in three well-aquifer system; the effect on gravity of the three waterlevel variations. In Vieira R (ed): *Proceedings 10'th Int. Symp. Earth Tides,* pp 843-854. Consejo Superior de Investigaciones Cientificas, Madrid.

Delcourt-Honorez M, 1991; Water level fluctuations in a borehole at the Royal Observatory of Belgium: Effects on local gravity, earth tides and barometric responses. In Kakkuri J (ed): *Proceedings 11'th Int. Symp. Earth Tides,* pp 389-412, Schweizerbart'sche Verlagsbuchhandlung, Stuttgart.

analyse tides and air pressure effects mostly for the purpose to study the well tide problem in conjunction with a sensitive gravimeter. The case in Brussels at the Royal Observatory, the site of a superconducting gravimeter (resolution 0.01 nm/s^2), is special to the extent that three water-rich aquifers underlie the station. Water table variations on the short term of less than 0.1 m are efficient to disturb the gravimeter at the 1 μGal (10 nm/s^2) level while the deeper aquifers act by deformation of a clay matrix and ensuing vertical displacement of the surface (typically 0.5 nm/s^2).

5.7 Applied Mathematics

R 5.7-1

Arfken G, 1985; *Mathematical Methods for Physicists.* Academic Press, San Diego, Cal., 3rd edition, 985 pp.

Special functions of mathematical physics, like Legendre polynomials. Potential theory, elasticity theory, vectors, tensors.

R 5.7-2

R 5.7-3

Mase G E, 1970; *Continuum Mechanics.* Schaum's Outline Series, McGraw-Hill, New York, N.Y., 221 pp.

Elasticity, tensor algebra.

R 5.7-4

R 5.7-5

Press W H, Teukolsky S A, Vetterling V T, Flannery B P, 1992; *Numerical Recipes. The Art of Scientific Computing. Cambridge University Press,* 2'nd ed., 963 pp.

Used here mainly for nonlinear least squares (Marquardt-Levenberg), confidence limits in the case of Student's, Chi-square, and Fisher distributions, eigenvalue problems (Jacobi-rotation).

R 5.7-6

IMSL-MATH library.

IMSL-SFUN library.

FORTRAN Subroutines for Mathematical Applications, Version January 1989. IMSL, Houston, Tx.

Used routines: Fast Fourier transforms of time series with lengths not an integer power of two.

5.7.1 Time series analysis with emphasis on tides

Venedikov A P, Arnoso J, Vieira R, 2001; Program VAV/2000 for tidal analysis of unevenly spaced data with irregular drift and coloured noise. *Proceedings 14th International Symposium on Earth Tides, J. Geod. Soc. Japan,* **47,** No. 1.

Venedikov A P, Vieira R, de Toro C, Arnoso J, 1997; A new program developed in Madrid for tidal data processing. *Bull d'Inform. Marées Terr.,* **126,** 9669-9704.

not seen.

R 5.7-7

Wenzel H-G, 1994; Earth tide analysis package ETERNA 3.0. *Bull. d'Inform. Marées Terr.,* **99,** 6813-6855.

Wenzel H-G, 1996; The Nanogal Software: Earth tide data processing package ETERNA 3.30. *Bull. d'Inform. Marées Terr.,* **124,** 9425-9439.

http://www-gik.bau-verm.uni-karlsruhe.de/~iagetc/eterna33.html

This is a standard analysis program. It can process very long time series and solves the tidal component by estimating admittance parameters for a number of wave-groups with least-squares. It can be obtained also by contacting Bernard Ducarme, Royal Observatory, Brussels, Belgium. The most recent version contains the Hartmann-Wenzel tide harmonic development.

Dwyer T E, Sylvester K A, 1991; A computer spreadsheet method for correcting aquifer test data for ocean tide influence. *Ground Water,* **29**, 750.

not seen. Seems very specialised.

5.7.2 General work on time series analysis

...that I have employed and found useful. Review comments hightlight this aspect rather than trying to give a general summary of the works.

R 5.7-8

Oppenheim A V, Shafer R W, 1975; *Digital Signal Processing,* Prentice-Hall, Englewood Cliffs, NJ, 505 pp.

Data filtering, transforms, auto-covariance, cross-covariance, windows, auto-power and cross-power spectra.

R 5.7-9

Jenkins G M, Watts D G, 1968; *Spectral Analysis and its Applications, Holden Day,* San Francisco, 525 pp.

Statistical description of data, covariance and spectrum estimates with confidence limits. Partial correlation. Covariance windowing.

R 5.7-10

Claerbout J F, 1976; *Fundamentals of Geophysical Data Processing,* McGraw-Hill, 274 pp.

Z-transform, filters, spectral factorisation methods (Toeplitz, Robinson, Whittle, Kolmogoroff), data modelling by least-squares, maximum entropy, adaptive filters, Levinson recursion; plus four chapters on seismic waves in layered media, which is outside the present scope.

R 5.7-11

Unbehauen R, 1971; Systemtheorie–Eine Einführung für Ingenieure. Oldenburg, München, 224 pp.

In German. Very useful sections on Fourier transforms and causality conditions, linear networks, phase space of systems etc.

6 Appendix B: Existing software

A flowchart of signals and computer programs is shown in Figure 6-1.

6.1 Tide analysis

The "***URTAP"*** program is developed in-house with a number of components acquired from international research institutes (governmental, university) and public literature.

The program consists of a set of data input/output procedures, digital filters, a tide synthesizer, a module for matrix inversion, maximum entropy filter, power spectrum computation, screen graphics display of time series and matrices, and a few additional tools to synthesize tides and explore parameter covariance *a posteriori*.

The present tide synthesizer is based on a routine by Büllesfeld (1985), which on the one-hand is somewhat outdated, but is difficult to replace. There is development needed to code up a more flexible program able to be linked with any of a whole suite of synthesizer modules.

The use of standard procedures in the tide community (stand-alone modules, e.g. ETERNA, Wenzel, 1996) has limitations for projects like the present. ETERNA for instance is focussed mostly on gravity and long time series. The URTAP program will make use of the tide synthesizer of the ETERNA package in the future. However, concerning signal conditioning and matrix inversion URTAP has a wider range of options.

A most prominent option for use in aquifers is the parameterised formulation of the fluid core resonance. Strain coupling coefficients estimated in post-processing procedures for fracture zone modelling are used to accurately describe the resonance curve inside the tidal wave groups in the diurnal band.

URTAP uses the Lanczos Generalised Inverse method (Aki and Richards, 1980) for matrix inversion. This has advantages for *a posteriori* analyses since the variance-covariance matrix of the least-squares problem has a convenient representation, and can be used to transform least-squares systems in subsequent, interpreting stages of analysis (less parameter bias, more realistic variance estimates).

URTAP interfaces with spectrum analysis routines that compute Wiener filters. This is useful when frequency-dependent response is important, like between air pressure and water level.

A user manual is available (written in HTML).

6.2 Tide synthesis

A FORTRAN-77 subroutine package "***Ttide***" for the computation of astronomical tide spectra and time series. Specialised on displacement and strain components. Written by H-G Scherneck 1990--, drawing from Büllesfeld (1985), and Wenzel (1994, 1996). Uses mostly the formulations of Wahr (1981), see also Scherneck (1991).

6.3 Ocean tide loading

A FORTRAN-77 main program "***olss***" and associated subroutine package "***Oload***" for the computation of ocean loading coefficients using the Green's function / point load convolution method. Written by H-G Scherneck 1993--. A related program, "***olfg***" is used to compute ocean loading parameters for the standards of the International Earth Rotation Service. HTML user manual pages are available.

6.4 Cross-spectrum signal analysis

A main program "***sasm06***" and a subroutine library "***sas***" has been coded up for cross-spectrum analysis following mostly Oppenheim and Shafer (1975) and Jenkins and Watts (1968). Includes Wiener filtering, Maximum Entropy method, and several options for data window and filter design. Fourier transform routines taken from IMSL library [R 3.6-4]

Partial correlation involving three simultaneous time series can also be carried out.

6.5 Fracture zone parameter determination

Some simple routines programmed in FORTRAN-77 using Numerical Recipes Levenberg-Marquardt algorithm to fit parameters in nonlinear relations with the least-squares condition. Two stages are implemented. First, the strain coupling coefficients (linear problem) and the parameters for the dissipative model are solved (nonlinear). The dissipative model is applied on the tidal admittance coefficients. Then, the fracture zone parameters are solved (nonlinear). In a last stage, predicted tide time series can be computed using the strain coupling coefficients.

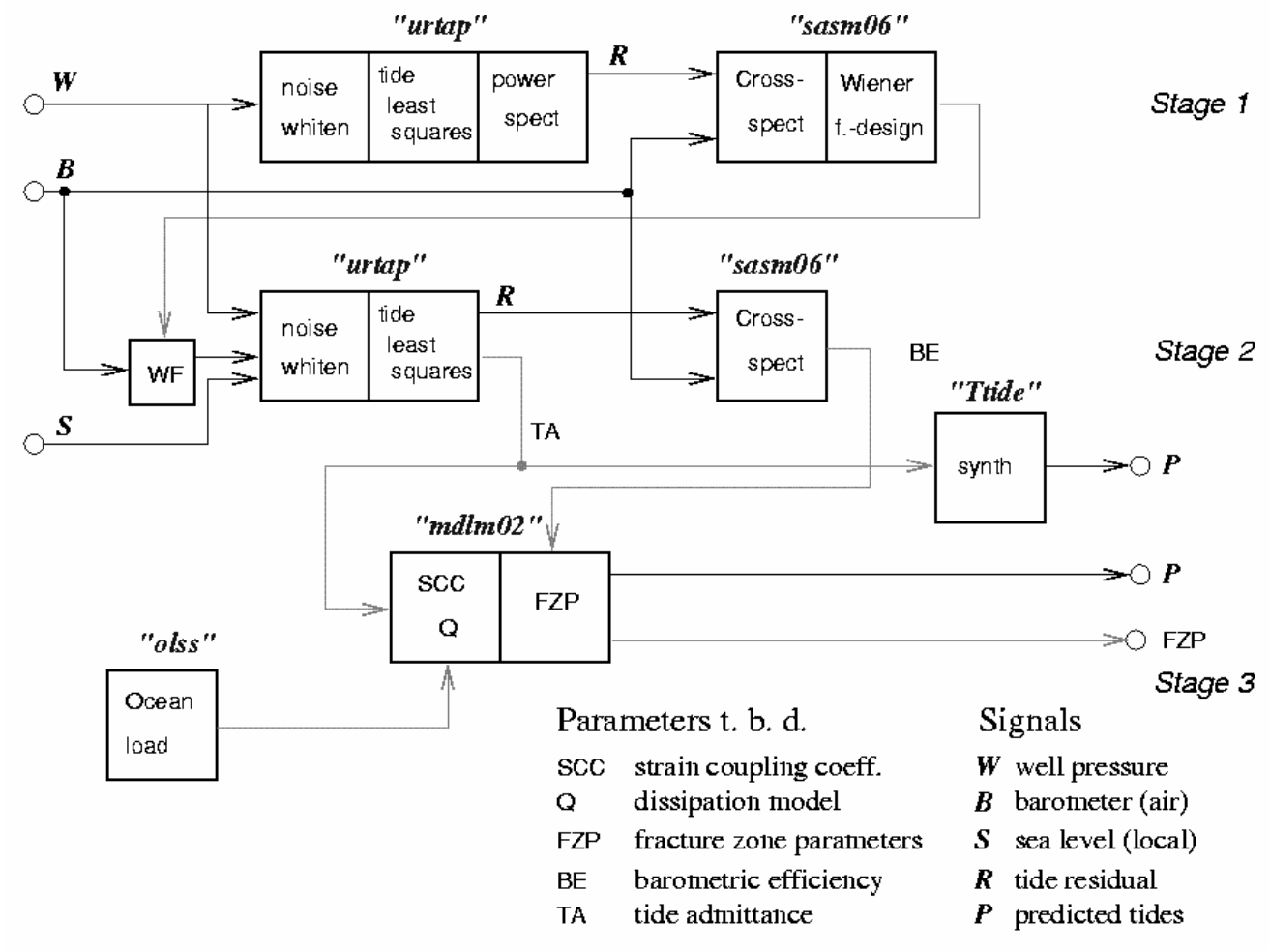

Figure 6-1. *Flowchart of signals and parameters through software modules*